Learning from Embryo Development to Engineer Self-organizing Materials

Anis Senoussi, Yuliia Vyborna, Hélène Berthoumieux, Jean-Christophe Galas, André Estévez Torres

Contents

Chapter 1

Learning from embryo development to engineer self-organizing materials

Authors. Anis Senoussi[1], Yuliia Vyborna[1], Hélène Berthoumieux[2], Jean-Christophe Galas*[1], André Estevez-Torres*[1]

(1) Laboratoire Jean Perrin and (2) Laboratoire de physique théorique de la matière condensée, Sorbonne Université and CNRS, 4 place Jussieu, 75005, Paris (France)

* jean-christophe.galas@upmc.fr, andre.estevez-torres@upmc.fr

In this chapter, we claim that concepts from embryo development are useful to engineer artificial out-of-equilibrium materials that self-construct. To this end, we consider embryo development as a process that brings a material from an initial state with low spatial chemical complexity and a high degree of chemical information —the equivalent of the egg— into a final state with high spatial complexity —corresponding to the developed organism. This process consumes chemical energy to convert chemical information into controlled changes in the composition and the shape of the material. In the quest of engineering such a

material, we focus on two fundamental steps of embryo development: pattern formation and morphogenesis. We discuss their basic mechanisms and provide examples of their implementation in synthetic systems.

Pattern formation refers to the self-organization of well-defined concentration patterns; it is linked to the dynamics of chemical reactions and controlled by reaction rates and diffusion. Morphogenesis concerns the implementation of controlled shape changes in a macroscopic material; it implies chemomechanical transduction pathways that generate mechanical forces at particular points of space. We start by introducing the basic features of embryo development and we argue how these can inspire the design of artificial self-organizing materials. Next, we review the two principal mechanisms of pattern formation: Turing patterns and positional information. Finally, we discuss reconstituted cytoskeletal active gels, a class of biochemical materials that generate forces and produce macroscopic shape changes by consuming chemical energy. The topic is highly multi-disciplinary and requires skills in physics, chemistry and biology. For this reason, we have attempted to provide the reader with the fundamental concepts from these fields needed to understand and engineer pattern formation and morphogenesis in artificial systems. The coupling between these two processes remains a fascinating challenge for the future.

1.1. The embryo is a material capable of chemical and morphological differentiation

The assembly of an artificial cell is a long-standing goal of bottom-up engineering, from chemistry to synthetic biology [9, 15]. It has been argued that such endeavor will help us, on the one side, to better understand living systems and, on the other side, to build autonomous microscopic entities capable of motion, division and information processing. As a complementary approach, in this chapter, we consider embryo development as a fruitful inspiration for the engineering of out-of-equilibrium materials that can self-construct in time and space.

From a physico-chemical point of view, embryo development is a fascinating process that converts a starting material with little spatial complexity into a highly differentiated final material. It is usually divided into four sequential processes [146] that are, however, commonly intertwined:

1. *pattern formation*, a process during which out-of-equilibrium molecular programs generate highly-ordered concentration patterns of μm to mm size, that chemically structure the embryo;
2. *morphogenesis*, where the embryo changes its shape due to internal and external cell movement promoted by molecular motors and filaments, as it happens during gastrulation;
3. *cell differentiation*, in which cells become structurally and functionally different; and
4. *growth*, resulting in an increase in the mass of the embryo.

Therefore, the embryo is structured by the interplay of chemical and physical forces. Pattern formation creates a blueprint of chemical species. Morphogenesis responds to chemical signatures generated by pattern formation but also to the mechanical constraints of the cell and tissue. Chemo-mechanical and mechano-chemical couplings link the two processes that, together, control cell differentiation and growth. In this chapter, we will focus on the first two steps: pattern formation and morphogenesis (Figure 1.1). It reduces the complexity of the problem while keeping the essential elements —chemical and morphological differentiation. We would like to warn the reader that this is a nascent field and thus our goal is not to provide a finished realization of an artificial embryo, but to suggest future directions from current knowledge. In particular, we will not provide experimental solutions to the essential problem of coupling pattern formation and morphogenesis, although we will point to possible implementations in the conclusion.

Because pattern formation is purely chemical, it is simpler to achieve in molecular systems than morphogenesis. There is a long history of research in the field of chemical pattern-forming systems, in particular patterns that are generated by the coupling of reaction and diffusion. We refer the interested reader to classical [26] and recent reviews [27] on this matter. Here, we will only consider chemical patterning inspired from development and thus two major conceptual frameworks will be discussed: Turing instability and positional information. The principal difference between the two is that the Turing instability is a symmetry-breaking mechanism that generates a heterogeneous state from a homogeneous one, while positional information is a sharpening mechanism that amplifies heterogeneity from an initial state where the symmetry has already been broken. The former will be treated in section 1.2 while the

latter will be discussed in section 1.3.

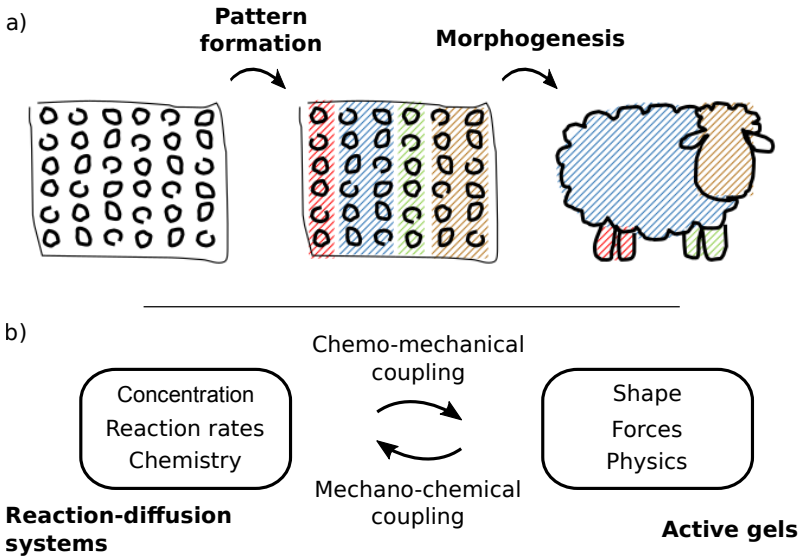

Figure 1.1: Embryo development as an inspiration for the development of self-organizing materials. a) Illustration of the two key phases of embryo development: pattern formation and morphogenesis. b) Scheme summarizing the interplay of chemical and physical processes that occur during the embryo structuration.

In both sections, we will provide a short theoretical introduction to the models behind both concepts. We will then briefly consider examples where these two mechanisms are observed in living embryos. Finally, we will review their experimental implementations in chemical and biochemical systems. Historically, redox reactions related to the Belousov-Zhabotinsky oscillator have been the system of choice to observe reaction-diffusion patterning and we will describe some examples. In addition, we will discuss the complementary biochemical implementations that have arisen in the last decade. In particular, purified Min protein waves, DNA/enzyme reaction networks, DNA hybridization reactions and systems based on transcription and translation.

Section 1.4 is dedicated to force generation and morphogenesis in molec-

ular systems. We believe that reconstituted systems that contain biological motors and filaments are a promising and important direction in this field. Thus, we have focused on these systems omitting other examples due to space limitations. We will first describe the physicochemical properties of their components. We will then introduce the hydrodynamic theory of active gels, that explains how chemical energy can be converted into mechanical force and material deformations. Finally, we will review recent experimental realizations of cytoskeletal gels in vitro, in particular those related to morphogenesis.

In the conclusion, we will consider the potential consequences that engineering materials inspired by embryo development might have in materials science and discuss the perspectives for coupling pattern formation and morphogenesis.

1.2. Pattern formation by a reaction-diffusion Turing instability

The first author to suggest that pattern formation in living systems may have a chemical basis was Alan Turing in 1952 [130, 129] in the landmark paper *The chemical basis of morphogenesis*.[1] Turing discovered that a mixture of chemical species that react and diffuse can, in some cases, generate an inhomogeneous concentration pattern from an initially homogeneous state and thus break the symmetry spontaneously. Such a mixture is called a reaction-diffusion (RD) system and the mechanism of symmetry-breaking receives the name of spatial instability. This instability happens only under the following necessary condi-

[1] For a historical perspective see ref. 3.

tions:

- the system requires at least two reactive species,
- concentration fluctuations need to be present in the initial homogeneous state,
- the diffusion coefficients of at least two species have to be different,
- the initial state should be stable in the absence of diffusion.

We stress that reaction-diffusion systems will only form concentration patterns if they are kept out of equilibrium.

The Turing instability is a complex concept. It is theoretically well understood for 2-component systems [91, 26, 92], but it is difficult to grasp for systems involving 3 [99] or more species [80, 115]. In a 1-dimensional spatial system, the Turing instability generates a periodic pattern sketched in Figure 1.2a. In 2 dimensions it generates dotted (Figure 1.2b) and labyrinthine patterns. In both cases, the wavelength of the patterns is given by $\sqrt{D/k}$, where k is a first-order reaction rate constant and D a diffusion coefficient.

The role of Turing patterns in the engineering of reaction-diffusion systems is similar to that of oscillators in the design of dynamic reaction systems: a strong experimental proof that one masters the underlying design principles. However, we will see that the Turing instability is more difficult to engineer in vitro, and to reveal in vivo, than the Hopf instability associated to oscillations. The rational design of Turing patterns has been, and still is, a far-reaching goal of systems chemistry [27, 154] and synthetic biology [112]. For this reason, we provide a succinct discussion of the theoretical conditions for observing a Turing instability in a 2-species system in the following section. Then, we review experimental observations of Turing patterns in vitro and in vivo. We conclude by discussing recent implementations of chemical waves, a reaction-

diffusion instability related to the Turing one.

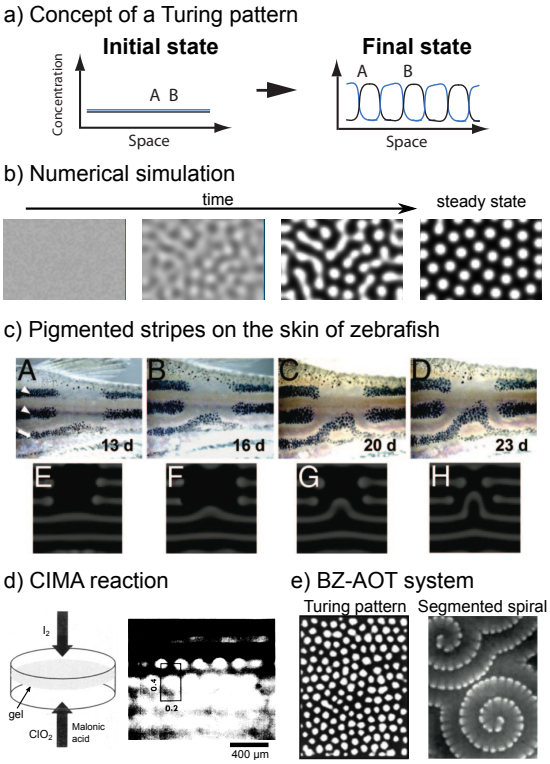

Figure 1.2: Pattern formation by a reaction-diffusion Turing instability. a) Sketch of a Turing pattern in 1 dimension. Note that the initial condition (left) presents concentration fluctuations necessary for the emergence of the patterns. b) Numerical simulation of a 2-species mechanism leading to Turing patterns in 2D, with $f([A],[B]) = k_1[A]^2/((1+K[A]^3)[B]) - k_2[A] + k_3$ and $g([A],[B]) = k_4[A]^2 - k_5[B] + k_6$ [58]. White color indicates high concentration of species A. c) Evidence of a Turing mechanism in the formation of pigmented stripes on the skin of zebrafish. Dynamics of pigmented stripes upon laser ablation (A-D, d = day). Reaction-diffusion simulations display similar dynamics (E-F). Adapted from [149], copyright (2007) National Academy of Sciences, USA. d) Turing patterns observed in the CIMA reaction. Left: scheme of the open gel reactor. The thin disk of gel, in gray, is connected to two open reactors on the top and bottom furnishing fresh reactants. Right: first experimentally-observed pattern. Adapted with permission from [68], copyright (1993) American Chemical Society and from [19], copyright (1990) American Physical Society. e) Examples of complex patterns obtained in the BZ-AOT system inside a closed reactor. Adapted from [27].

1.2.1. Short mathematical analysis of the Turing instability in a 2-species system

We consider two reactive species A and B. In the absence of diffusion, for example in a well-stirred reactor, the evolution of the concentrations $[A]$ and $[B]$ can be written

$$\frac{\mathrm{d}[A]}{\mathrm{d}t} = f([A],[B]) \tag{1.1}$$
$$\frac{\mathrm{d}[B]}{\mathrm{d}t} = g([A],[B]), \tag{1.2}$$

where f and g are functions accounting for reaction kinetics.[2] We will call this the 0-dimensional, or 0D case. In a non-stirred 1-dimensional reactor, diffusion has to be taken into account and we have to consider the equations

$$\frac{\partial[A]}{\partial t} = f([A],[B]) + \frac{\partial^2[A]}{\partial x^2} \tag{1.3}$$
$$\frac{\partial[B]}{\partial t} = g([A],[B]) + D\frac{\partial^2[B]}{\partial x^2}, \tag{1.4}$$

where diffusion coefficients of A and B are 1 and D, respectively, and diffusion is allowed in the x direction. We will call this the 1D case.

The Turing instability arises when the steady-state is stable in 0D to small perturbations in the concentrations but unstable in the presence of diffusion (1D case); it is a diffusion-driven instability. The steady states $([A]_{ss},[B]_{ss})$ of the 0D system correspond to the solutions of (1.1-1.2) when the left-hand side is equal to zero. The stability of the steady states of the 0D and 1D system is

[2] For instance, if we consider the elementary reaction $A + B \xrightarrow{k} 2A$, $f([A],[B]) = 2k[A][B]$ and $g([A],[B]) = -k[A][B]$.

evaluated using linear stability analysis [26], a method that looks at the effect of small perturbations around the steady state. This method uses the Jacobian matrix associated to (1.1-1.2), defined as

$$J = \begin{pmatrix} \frac{\partial f}{\partial [A]} & \frac{\partial f}{\partial [B]} \\ \frac{\partial g}{\partial [A]} & \frac{\partial g}{\partial [B]} \end{pmatrix}_{ss} = \begin{pmatrix} f_A & f_B \\ g_A & g_B \end{pmatrix}_{ss}, \tag{1.5}$$

where the index ss indicates that the Jacobian is evaluated at the steady state $([A]_{ss}, [B]_{ss})$ and thus f_A, f_B, etc. are not functions but numbers. This is a crucial point that renders very complex the rational design of a reaction network producing Turing patterns —see below. The 0D system is stable around the steady state if and only if

$$\mathrm{tr}(J) = f_A + g_B < 0 \qquad \text{Condition 1} \tag{1.6}$$

$$\det(J) = f_A g_B - f_B g_A > 0 \qquad \text{Condition 2} \tag{1.7}$$

and the 1D system is unstable around the steady state, for at least one wavelength, if and only if

$$D f_A + g_B > 0 \qquad \text{Condition 3} \tag{1.8}$$

$$(D f_A + g_B)^2 > 4D(f_A g_B - f_B g_A) \qquad \text{Condition 4.} \tag{1.9}$$

A Turing instability can thus just be observed if all the four conditions (1.6-1.9) are verified. An example is given in Figure 1.2b.

The first three Turing conditions (1.6-1.8) have a clear physical meaning. Conditions 1 and 2 impose the signs of the Jacobian compatible with Turing. If we suppose $f_A > 0$, meaning that species A is an autocatalyst, the only

possibilities are

$$\begin{pmatrix} + & - \\ + & - \end{pmatrix}, \quad \begin{pmatrix} + & + \\ - & - \end{pmatrix}. \tag{1.10}$$

The signs of the Jacobian define the topologies of the reaction networks, *i.e.* the mechanisms, that are compatible with the Turing instability. The left-hand sign matrix is associated with an activator-inhibitor network and the right-hand one with a so-called substrate-depleted network.

Conditions 1 and 3 impose $D > 1$, which means that B has to diffuse faster than A. In addition, the larger the value of D, the easier it will be to verify condition 4 if conditions 1 and 3 are respected. Being more intuitive than conditions 1-4, the constraints associated with the signs of the Jacobian matrix (1.10) and with $D > 1$ have been extremely influential in the history of Turing patterns. They were summarized by Gierer and Mienhardt [32, 83] in the *motto* 'short-range activation and long-range inhibition'[3]. However, it is important to point out that (1.10) and $D > 1$ are necessary but not sufficient conditions to obtain a Turing instability in a 2-species system. As a consequence, Meinhardt's *motto* has been recently criticized [80, 39].

What remains true, however, is that the four Turing conditions (1.6-1.9) impose strong constraints on the values of the Jacobian elements, which are directly controlled by the underlying reaction network. Moreover, they require a difference in diffusion between two species. The rational design of Turing-compatible reaction networks implies mechanisms associated with functions f and g that are compatible with conditions 1–4. The difficulty is that the constraints imposed on functions f and g are hidden in the requirement that

[3]Also known as local auto-activation and lateral inhibition (LALI).

conditions 1–4 must be verified at steady state. For example, changes in the values of the reaction rate constants, or in the mechanism of the reaction, will result in simultaneous changes in the steady-state of the 0D system and in the functional form of the Jacobian, thus affecting conditions 1–4 in an unpredictable way.

1.2.2. Turing patterns in vivo

In developmental biology, Turing ideas have been as influential as they have been criticized [36]. Predominant in the 1970s and 80s, the observation of positional information patterning in the fruit fly in the end of the 1980s (see below), largely discredited Turing patterns among developmental biologists. However, this idea is recently regaining importance [60]. In 1995, Kondo and Asai suggested that a Turing model could explain why the stripe patterns on the surface of the tropical fish *Pomacanthus imperator* moved on the scale of days [59]. A similar observation was made later for the stripe patterns on the skin of zebrafish, that moved with dynamics compatible with a Turing instability upon laser ablation (Figure 1.2c) [149]. Evidence of an underlying Turing mechanism has also been reported during the formation of the periodic ridges in the palate [24] and during digit patterning, [114] both in mice.

1.2.3. Turing patterns in vitro

Turing patterns were observed for the first time in vitro in 1990 by de Kepper and colleagues in the chlorite-iodide-malonic acid reaction (CIMA), almost 40 years after Turing's discovery (Figure 1.2d). Experiments were carried in a thin disk of gel which upper and lower sides were connected to open reactors in order

to keep the system truly out of equilibrium. The gel suppressed convection and thus allowed the observation of RD phenomena. In addition, the reaction was performed in the presence of starch, initially used as a color indicator for I_3^- ions, but also playing a crucial role in modifying the effective reaction and diffusion rates of I^-, and helping to satisfy the Turing conditions just evoked.

Shortly after, a theoretical explanation of why the CIMA reaction produces Turing patterns was provided by Lengyel and Epstein [66, 67, 68]. Importantly, these authors explained how the addition of an immobile species binding to the activator enlarges the Turing space of parameters.

Starting in 2001, Vanag and Epstein published a series of remarkable observations of complex RD patterns in a closed reactor. They did so by devising a clever strategy to strongly reduce the diffusion coefficient of some reactants in the Belousov-Zhabotinsky (BZ) oscillator. More precisely, the BZ reaction was dispersed inside water-in-oil droplets stabilized by the surfactant aerosol OT (AOT[4]). The water droplets had a well-defined diameter that could be tuned between 1 and 10 nm. The advantage of this reaction medium is that hydrophilic BZ species are retained inside the droplets whereas hydrophobic ones can freely diffuse from droplet to droplet across the oil phase. As a result, hydrophobic species, such as Br_2 or $BrO_2^\bullet$, diffuse fast, with $D = 10^{-9}$ m^2s^{-1}, while the diffusion of hydrophilic species, such as Br^-, is limited by the diffusion of the droplets, typically $10^{-11} - 10^{-12}$ m^2s^{-1}. Finally, the observation of patterns is facilitated because the BZ reaction can be kept out of equilibrium in a closed reactor for long periods of time. In this system the authors observed Turing patterns, [139] but also, antispirals [137] (Figure 1.2e), segmented spirals, [138] standing waves [5] and Turing patterns in 3-dimensions [4]. Later, a

[4]Aerosol sodium bis(2-ethylhexyl) sulfosuccinate.

more controlled version of this system was obtained using microfluidics. [125]

Between 1990 and 2009 Turing patterns were observed in just 2 different chemical systems, showing the great difficulty of engineering a Turing instability. Patterns in the CIMA reaction were obtained by chance and patterns in the BZ-AOT system were observed by designing the diffusion terms but relying on the well-known BZ oscillator. In 2009, de Kepper and colleagues were able to rationally design Turing patterns in the thiourea-iodate-sulfite reaction system [42]. Their strategy could inspire current efforts of engineering Turing patterns in more controllable systems, such as DNA reactions [136] or synthetic biology [112].

1.2.4. Simpler than Turing: reaction-diffusion waves in vitro

Turing patterns in vitro have only been observed with redox reactions involving small molecules. Besides their advantages, these systems display two important drawbacks. Firstly, they are not programmable, which means that one cannot rationally design the reaction mechanism. Secondly, they are not biocompatible as the reaction requires strong acidic conditions. Programmability is important for the rational design of out-of-equilibrium materials that display precise RD patterns. Biocompatibility is necessary for the coupling of RD to biochemical and biological systems such as proteins and living cells. The development of programmable and biocompatible reactions that generate reaction-diffusion systems has been an important quest in the field in the last 15 years.

In the following, we focus on two reaction-diffusion systems that are biocompatible and programmable to some extent. Although Turing patterns have

not been observed with them, they are prone to a related reaction-diffusion instability: wave propagation. The first one is an in vitro implementation of the Min protein system, which positions the division machinery in some bacteria. The second one emulates a predator-prey oscillator using short oligonucleotides and DNA-dependent enzymes.

1.2.4.1. Min protein waves

Before they divide, cells must calculate the position where division will take place. In bacteria, this process is triggered by the polymerization of protein FtsZ into a structure called the Z-ring. In bacteria such as *E. coli*, division happens at the midpoint of the cell with 3% accuracy [76]. This accuracy is reached thanks to the computation abilities of two processes, nucleoid occlusion and Min oscillations.

The Min system is one of the best studied reaction-diffusion systems in living cells. It is composed of three proteins MinC, MinD and MinE, which intracellular dynamics inhibit cell division at the poles and promote the formation of the Z-ring at the center [76]. The mechanism is depicted in Figure 1.3a and consists of 5 steps. Free-diffusing MinD-ADP is phosphorilated into MinD-ATP (1), triggering its dimerization and binding onto the membrane (2). MinC and MinE can both bind to membrane-bound MinD (3-4), with MinE dephosporilating bound MinD and regenerating free MinD-ADP (5).

In vivo, MinC and MinD concentrations at the membrane continuously oscillate from pole to pole, forming a standing wave of period ~ 1 min. [105] At the same time, MinE forms a ring at the frontier between high and low MinC/MinD surface concentration. MinD and MinE are needed for oscillations

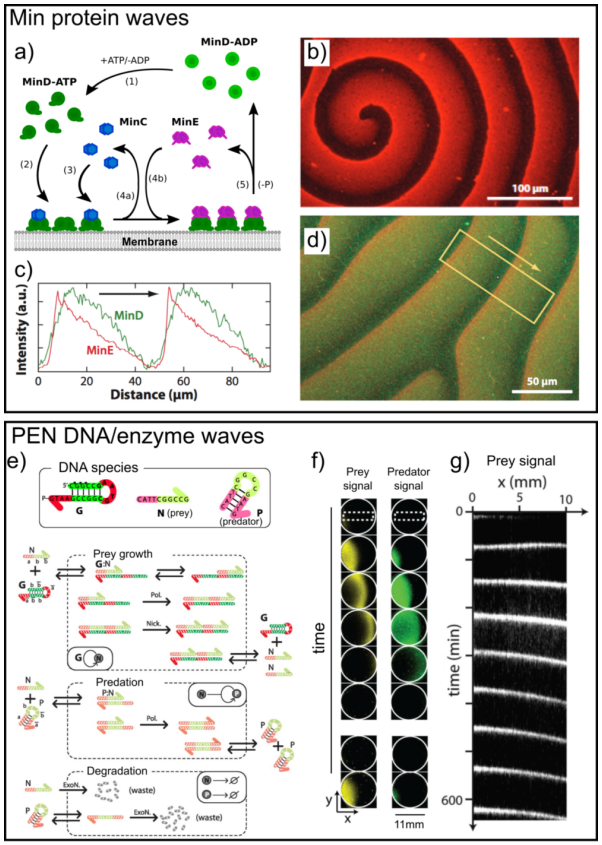

Figure 1.3: In vitro reaction-diffusion waves using two different systems: a purified Min protein system (a-d) and a semi-synthetic DNA/enzyme system (e-g). a) Mechanism of the Min system [76], see text. Spiral pattern of MinE (b) and waves of MinD, followed by MinE, (c-d) observed in vitro on a supported lipid bilayer. Panel c displays fluorescence intensity profiles inside the rectangle on (d). e) Mechanism of a predator-prey mechanism implemented with PEN reactions. DNA sequences of the 3 species (N, prey, P, predator, G, template for the production of N) and details of the 3 reactions, see text. Complementary DNA domains have the same color. The polymerase, nicking enzyme and exonuclease are noted Pol, Nick and ExoN, respectively. f) Time-lapse images of the yellow fluorescence signal (corresponding to [N]) and the green channel (corresponding to [P]), taken every 10 min in an 11 mm diameter circular reactor (in white). g) Kymograph of the yellow fluorescence (corresponding to [N]) along x over 600 min. Adapted with permission from [75] (b-d) and from [29, 101], Copyright (2013) American Chemical Society (e-g).

but not MinC [44].

Loose, Schwille and co-workers observed in 2008 Min oscillations in a reconstituted in vitro system [75]. In the presence of ATP and a lipid bilayer supported on glass, fluorescently-labeled MinE and MinD generated spiral patterns and traveling concentration waves on the surface of the membrane (Figure 1.3 a-d), with typical velocities of 30 μm/min and wavelengths of 50 μm. The in vitro wave speeds are comparable to in vivo ones and are determined by the ratio between the concentrations of MinE and MinD. [76] Also, MinE accumulates behind the MinD wave, as observed in vivo. However, the in vitro wavelengths are 10-fold larger than those observed in vivo.

In summary, this in vitro model is a unique framework to investigate how proteins can self-organize to form patterns, including the role of confinement.

1.2.4.2. DNA/enzyme waves

The Min system has the singularity of requiring one of the species to bind to a surface to generate a traveling wave. In the absence of surface binding, a chemical wave can be generated by an oscillator in the presence of diffusion. There are several implementations for an oscillator, but one that is particularly robust is the predator-prey mechanism, that was introduced theoretically by Lotka [78] and Volterra [142] at the beginning of the 20th century at the crossroads of chemistry and population dynamics. Predator-prey dynamics rely on three basic dynamic interactions: i) a prey population that grows exponentially in the absence of predator, ii) a predator population that consumes prey and grows exponentially and iii) the continuous destruction of both populations.

These three processes can be interpreted as three reactions involving two chemical species, prey and predator. They were implemented for the first time

in a chemical system by Fujii and Rondelez in 2013 [29] using oligonucleotides and enzymes in a reaction framework called the PEN DNA toolbox [87, 2]. PEN refers to the three enzymes that are involved in the reaction: polymerase, exonuclease and nicking enzyme. Following DNA hybridization rules, the sequence of the single stranded DNA (ssDNA) species define the topology of the reaction network while enzymes produce or degrade ssDNAs.

The mechanism of the DNA/enzyme predator-prey (PP) oscillator is detailed in Figure 1.3 e. During prey growth ($N + G \rightarrow 2N + G$), the 10 base-long prey strand, noted N, replicates autocatalytically on template G, a 20 base-long ssDNA whose sequence is twice complementary to N. A polymerase and a nicking enzyme are involved in the reaction, as well as deoxyribonucleotides (dNTPs) that are consumed by the polymerase to synthesize N. In the predation reaction ($P + N \rightarrow 2N$), the 14 base-long predator, noted P, grows autocatalytically consuming the prey. The trick is that species P is both self-complementary and contains the sequence of N. Thus, when P and N bind together and the polymerase extends N, we obtain two copies of P. In addition, these strands are continuously degraded by exonuclease, while chemically-protected strand G remains intact. Concentrations of N and P are measured by fluorescence.

In a well-mixed and closed reactor, the mixture of N, P, G and the three enzymes produces oscillations in the concentrations of N and P with a period $\sim$ 100 minutes that last for tens of hours [29]. Inside a thin circular reactor, where mixing is only possible by diffusion, the same mixture generates traveling concentration waves of N, followed by waves of P. Wave velocities are in the range of 80-400 μm/min, and more than 10 successive waves crossing the entire reactor can be observed (Figure 1.3 f and g) [101]. This experiment constituted

the first rational design of predator-prey waves in the laboratory.

To the best of our knowledge, the Min and PEN DNA reaction-diffusion systems have not been adjusted to meet the Turing criteria. Nevertheless, the programmability [153] and the biocompatibility of the biochemical species involved here open up new perspectives for the engineering of increasingly complex spatio-temporal reaction-diffusion patterns that may be coupled to morphogenesis [71, 154].

1.3. Pattern formation by positional information

The Turing instability discussed in the previous section is a symmetry-breaking mechanism. In many situations during embryo development, however, patterning happens from an already heterogeneous initial condition, typically a concentration gradient of a protein or an mRNA. Lewis Wolpert in 1969 proposed a conceptual framework [147] to explain how an embryo with a single break of symmetry (induced through a Turing process or by a maternal gradient) could differentiate further into several distinct regions. He proposed the term 'French flag problem' to illustrate the challenge —pervasive in the development of virtually all complex organisms— of generating distinct regions of space with sharp borders from an amorphous mass and a shallow concentration gradient.

Wolpert's idea makes it easy to visualize, albeit in a simplistic way, how a morphogen gradient spread within an embryo can be used to define the fate of the embryo's cells. How will the cells on the left become the head, the cells on the right the abdomen and the cells in the middle the thorax? Simply by

reading a concentration. As depicted in the Figure 1.4a, each cell may define its fate by simply measuring the morphogen concentration around itself. Two concentration thresholds, M_1 and M_2, will then be sufficient to provide three cell fates. The gradient thus provides to the cells what is called a *positional information*.

In contrast with Turing's, Wolpert's idea is not a mechanism but a useful conceptual framework, because it does not provide details about how the cells read out the corresponding thresholds. Initially [147, 36], Wolpert argued that positional information and Turing instability were mutually exclusive, the latter happening through a reaction-diffusion mechanism in contrast with the former [36]. These point of view is now being criticized among developmental biologists with two arguments: i) that positional information and reaction-diffusion are complementary mechanisms [36] that can be employed hierarchicaly during pattern formation —for example, a Turing mechanism could generate the morphogen gradient necessary for positional information— and ii) that positional information may be more robust if it happened through a reaction-diffusion mechanism [104]. Patterns generated by positional information were first observed in vivo and later in vitro. In the following, we will first describe models attempting to explain how thresholds could be read out by chemical processes. We will then summarize experimental evidence of positional information, first in vivo in *Drosophila*, and later in vitro.

1.3.1. Models of positional information

The key goal of these models is to generate a threshold (binary) response from a continuous input gradient of morphogen. Three chemical mechanisms have

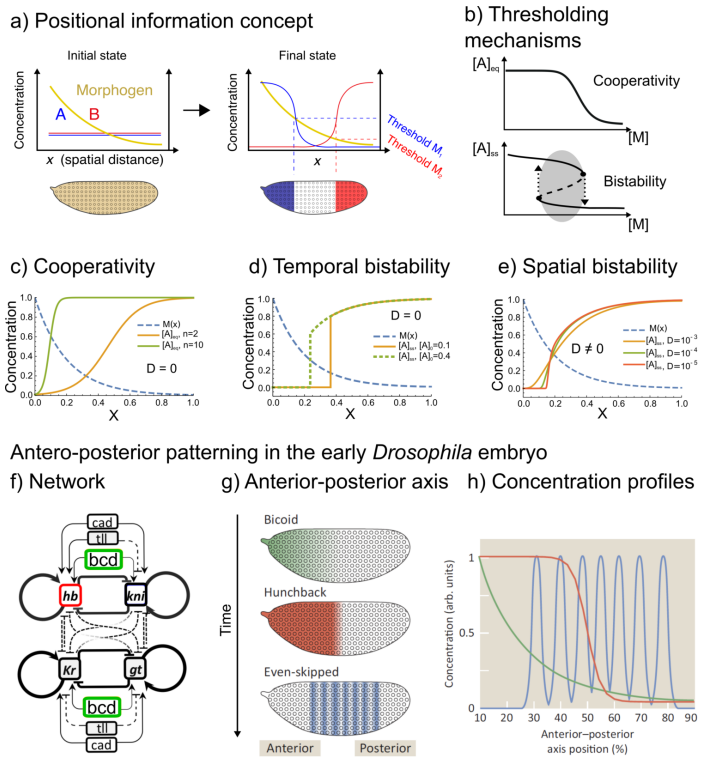

Figure 1.4: Concept, models and in vivo data of patterning by positional information . a) Illustration of Wolpert's concept as a solution of the 'French flag problem'. b) Schemes of two mechanisms inducing a threshold response in concentration of A from a continuous variation of [M]: cooperativity and bistability. c-e) Behavior of the three associated spatial models in the presence of identical gradients of morphogen M (dashed line). c) $[A]_{eq}$ is given for two values of the cooperativity factor n in equation (1.12). d) $[A]_{ss}$ for two different values of $[A]_0$ in equation (1.13). (e) $[A]_{ss}$ for different diffusion coefficients D in equation (1.14). f-h) Patterning genes in the early Drosophila embryo [50]. Gap gene regulatory network (bcd:bicoid, cad:caudal, hb:hunchback, Kr:Kruppel, kni:knirps, gt:giant, tll:tailless) (f). Patterning genes along the anterior-posterior axis. Chronologically, sketches showing protein concentrations of: the maternal genes (e.g. Bicoid, in green), the gap genes (e.g. Hunchback, in red) and the pair-rule genes (e.g. Even-skipped, in blue) (g). Corresponding concentration profiles (h). Adapted from [37] with permission from Elsevier (g,h).

been proposed that are compatible with this behavior:

1. equilibrium models based on cooperativity,
2. non-equilibrium models based on reaction-only bistability, and
3. non-equilibrium models based on reaction-diffusion bistability.

We discuss them briefly in the following.

1.3.1.1. Equilibrium model: cooperativity

The first possibility is to consider a species A that binds cooperatively with morphogen M. Thresholding is here viewed as an equilibrium process. We thus write the reaction

$$\mathrm{A} + n\mathrm{M} \rightleftharpoons \mathrm{AM}_n \qquad K = \frac{[AM_n]_{eq}}{[A]_{eq} \cdot [M]_{eq}^n} \tag{1.11}$$

with association constant K and cooperativity n, the index eq denoting concentrations at equilibrium. Using (1.11) we have

$$[A]_{eq} = \frac{[A]_0}{1 + K \cdot [M]^n}, \tag{1.12}$$

where $[A]_0$ is the total concentration of A. The equilibrium concentration of free species A, $[A]_{eq}$, is a sigmoidal function of $[M]$ that becomes steeper as cooperativity n increases (Figure 1.4b). If M is distributed along the x spatial axis as a decreasing exponential function $[M](x) \sim [M]_0 e^{-x}$, and diffusion is zero, this model provides concentration profiles of free species A as in (Figure 1.4c). As expected, the output profiles are steeper as n increases, but a clear threshold does not exist. Currently, we consider that this in vivo model is not enough to provide positional information, but it certainly contributes to

one of the models below[5].

1.3.1.2. Reaction-only mechanism: temporal bistability

A second possibility is to consider that A is involved in a non-equilibrium bistable reaction network, where the morphogen M plays the role of a bifurcation parameter. Many bistable functions can be proposed. For convenience, we will illustrate this model with a function describing one of the PEN DNA bistable networks described in section 1.3.3.2 [88]. In this case, M is a repressor species and the evolution of A is provided by the following differential equation

$$\frac{\mathrm{d}[A]}{\mathrm{d}t} = f([A]) = \frac{[A]}{1+[A]} - k_m \frac{[M]\cdot[A]}{K_m+[A]} - k_d[A]. \tag{1.13}$$

The three terms on the right-hand side of this equation account for A being an autocatalyst, M repressing A and A being linearly degraded, respectively, and k_m, K_m, and k_d are parameters. The behavior of the temporal bistable is given by the steady-states of (1.13), found when $f([A]) = 0$, which can take three different values $[A]_{ss}$. For a given set of parameters, the concentration of species M behaves as a bifurcation parameter of (1.13). This means that varying [M] changes the stability of the three steady-states $[A]_{ss}$. This is a very good way to make thresholds, because only stable steady-states will be reached. Figure 1.4b (bottom) plots the stability of the three steady-states as a function of $[M]$. If the morphogen is again exponentially distributed and diffusion is zero, a temporal bistable produces infinitely steep profiles of A (Figure 1.4d). However, the position of the profiles along x is very sensitive to

[5]Because the transcription factors involved in *Drosophila* patterning such as Bicoid, see below, are strongly cooperative.

the initial concentration, $[A]_0$, of species A.

1.3.1.3. Reaction-diffusion mechanism: spatial bistability

The last model couples temporal bistability with diffusion. In this case we should consider the equation

$$\frac{\partial [A]}{\partial t} = f([A]) + D\frac{\partial^2 [A]}{\partial x^2}, \tag{1.14}$$

where $f([A])$ is the kinetic function given in (1.13) and D the diffusion coefficient of A. This model still provides steady-state profiles $A_{ss}(x)$ that are very steep when D is small (Figure 1.4e). Interestingly, diffusion makes gradient interpretation through a bistable network more robust because the position of the A profile along x is insensitive to the initial concentration, $[A]_0$, of species A [107, 104].

1.3.2. Positional information in vivo: patterning of the Drosophila blastoderm

The first clear evidence of positional information was observed during the early development of the fruit fly *Drosophila melanogaster*, which is one of the best studied model organisms. In the following, we will discuss briefly pattern formation in this organism with two objectives: provide some biological ground for the engineering of an artificial embryo and assess the validity of the models just evoked.

In *Drosophila*, the complete growth process from egg to adult takes approximately 10 days and it involves four distinct stages: embryo, larva, pupa and

adult. Embryogenesis lasts only 24 h, after which the egg hatches into a larva [146]. *Drosophila* embryogenesis is singular among model organisms in that it initially takes place in a syncytium, a single cytoplasm where nuclei divide without cell membranes, which could facilitate morphogen transport by diffusion. During these stages, the embryo is called a syncytial blastoderm, with the yolk occupying a large central part and the cortex containing a monolayer of nuclei. The blastoderm —a 500 μm long ovoid — has two hierarchical systems of patterning, an antero-posterior and a dorso-ventral. We will discuss here the former.

Positional information during antero-posterior patterning is provided by three maternally-induced protein gradients. One of them is Bicoid, whose concentration decreases gradually from the anterior to the posterior of the embryo (from left to right in Figure 1.4g, top) [49, 50]. These gradual maternal gradients regulate the expression of downstream gap genes that produce sharp concentration profiles of their protein products. For example, the Bicoid gradient generates a sharp Hunchback gap profile (Figure 1.4g, center). There are, however, more than twelve gap gene proteins [37]. Subsequently, gap and maternal proteins control the formation of pair-rule protein patterns, such as Even-skipped, that form seven 50 μm-wide stripes that will help define the positions of body segments that form later in development (Figure 1.4g, bottom).

In the last decades, several models have tried to explain pattern formation in the *Drosophila* blastoderm, Turing and positional information being the main ones [49]. Since the work of Driever and Nüsslein-Volhard in 1988 [23, 22], positional information has been favored by experimental data; although a vivid debate remains concerning its mechanism, in particular the role played by diffusion. Experimental data of protein expression in *Drosophila* come principally

from immuno-staining of protein products in fixed embryos. As a result, to get a dynamic picture of patterning one needs to fix different embryos at sequential time-points, introducing potential artifacts. Jaeger and coworkers concluded that a model related to temporal bistability, in the absence of diffusion, fits best these type of data [51, 49]. Although, the underlying reaction network is relatively complex: it involves three maternal genes and four gap genes that activate and repress each other (Figure 1.4f). In contrast, other works suggest that the formation of Hunchback's sharp profile is compatible with a spatial bistability mechanism and thus would need diffusion [77]. In addition, recent theoretical arguments suggest that diffusion of gap proteins can stabilize the boundaries of gap concentration profiles in the presence of fluctuations [104]. The cooperativity model is not anymore considered to be central to provide thresholding in positional information. However, cooperativity is believed to play an important role in steepening the response of the reaction network involved [65]. Finally, patterning by positional information has been observed beyond *Drosophila*, notably during the patterning of the vertebral neural tube [14].

1.3.3. Positional information in vitro

As we have seen, in vitro implementations of reaction-diffusion Turing patterns are scarce because the Turing constraints are difficult to meet experimentally. In contrast, positional information generates robust concentration patterns in vitro. In the following, we will detail three biochemical systems that produce such patterns. The first one relies on DNA-hybridization reactions, the second one involves PEN DNA/enzyme reactions and the last one takes advantage of

a cell-free transcription-translation system.

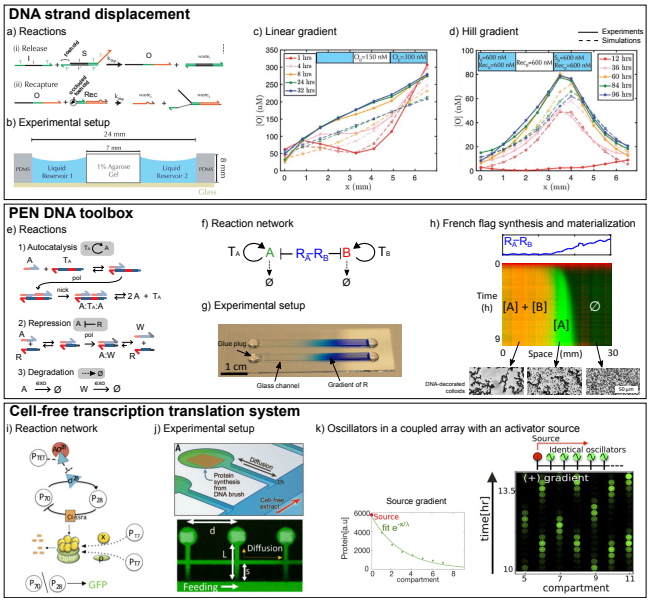

Figure 1.5: Experimental patterns of positional information in vitro with three systems: DNA strand displacement (top), PEN DNA/enzyme (center) and cell-free transcription-translation (bottom) reactions. DNA strand displacement reactions (-d). a) Reaction mechanism: fast release (i) and slow recapture (ii) of the output strand O. b) Experimental setup. Two liquid reservoirs (containing solutions of DNA) separated by an agarose hydrogel. c-d) Pattern formation: linear gradients (c) and stable hill gradients (d) are formed depending on initial concentrations (shown in the insets). PEN reactions (e-h) [154]. e) Reaction mechanism of a bistable network. f) A tetrastable network combining two orthogonal bistable networks. g) Experimental setup. A sealed rectangular glass capillary that contains a uniform solution of all species except a gradient of repressor (in blue). h) French flag synthesis and materialization. The reaction network in (f) reads and interprets a pre-existing gradient of R_A-R_B (in blue) to generate 3 chemically-distinct zones (A+B, A and $\emptyset$) that induce DNA-coated beads aggregation (bottom). Cell-free system (i-k). i) Activator-repressor network. σ28 is the activator, CI the repressor. j) Experimental setup. Circular compartments with a DNA brush for protein synthesis are coupled through channels. k) Kymograph (GFP fluorescence over space and time) in an array of coupled oscillators subjected to an underlying gradient of activator. Adapted from [156] (a-d), published by The Royal Society of Chemistry and from [123], copyright (2017), National Academy of Sciences USA.

1.3.3.1. DNA strand displacement patterns

DNA strand displacement (DSD) is a hybridization reaction involving single and partially double stranded DNAs that can be used to construct digital (e.g. logic gates) and analog (e.g. oscillators) chemical circuits [152, 158]. This reaction framework has the advantage of being fully programmable because association and dissociation rates can be predicted from the sequence [128, 157]. However, DSD reaction networks are harder to maintain out of equilibrium [117] than those built from PEN reactions [29], for instance.

Zenk, Schulman and co-workers used DSD reactions to implement positional information patterns (Figure 1.5 top panel). They first generated a smooth morphogen gradient by diffusion, with a source-sink mechanism between two reservoirs separated by a convection-free zone (Figure 1.5b,c). Coupling two of these gradients to a release and recapture mechanism they obtained a hill-shaped pattern of DNA at steady state. Note that this mechanism is different from those described in 1.3.1 in that it needs a spatial open reactor to generate a stable pattern.

The mechanism is sketched in Figure 1.5a. In the release reaction $\mathrm{I} + \mathrm{S} \rightarrow \mathrm{O} + \mathrm{W}_1$, I is an ssDNA and S a partially double strand complex with a single stranded side called toehold. I binds to the toehold of S and releases ssDNA O, the patterning species, and dsDNA W_1, a waste molecule. The recapture reaction $\mathrm{O} + \mathrm{Rec} \rightarrow \mathrm{W}_2 + \mathrm{W}_3$, follows a similar scheme but the toehold where O binds to Rec is occluded and thus the recapture rate is much slower that the release rate.

The combination of rapid creation and slow degradation of O allows the authors to generate a hill gradient of O from two underlying gradients of I and S using a 1D open reactor (Figure 1.5b). To do so, two opposite source-

sink gradients are created by diffusion, simply adding strand I only in the left reservoir and strand S only in the right reservoir. The concentration of Rec strand is uniform throughout the device and [O] is recorded over time by fluorescence. 30 hours are necessary for the formation of the final hill-shaped gradient, which lasts about 70 hours (Figure 1.5d). To keep the system out of equilibrium for such a long time, the solutions in the lateral reservoirs are renewed every 24 hours.

DNA strand displacement reactions only rely on DNA strands. They offer robustness and programmability, making the method a great route to explore other reaction-diffusion patterns, beyond the positional information framework [143, 136].

1.3.3.2. PEN DNA/enzyme patterns

In 1.2.4.2 we described the engineering of predator-prey oscillations and waves using PEN reactions. In this framework, the design of reaction networks depends on DNA hybridization rules and can thus be rationalized. In contrast, catalysis depends on DNA-dependent enzymes. Enzymes provide specificity and a simple way to keep the network out of equilibrium by the slow consumption of chemical energy from dNTPs, but they introduce a source of variability that cannot be fully rationalized. PEN reactions have been recently used to demonstrate a series of temporal [87, 29, 100, 88] and spatiotemporal pattern [101, 153, 155, 154, 132]. Here, we will describe the experimental implementation of a French flag pattern of positional information using a spatial bistability mechanism [154] (Figure 1.5, central panel).

As described earlier, spatial bistability generates two chemically distinct zones separated by a sharp border from a morphogen gradient and a bistable

network whose bifurcation parameter is the morphogen concentration [107].

Figure 1.5e represents three PEN reactions that encode a bistable system [88]: i) the autocatalytic production of A mediated by template T_A ($A + T_A \rightarrow T_A + 2A$), which is similar to prey growth; ii) the nonlinear degradation of A mediated by repressor strand R (A+R→W+R, W a waste strand), called repression and related to predation but with a non self-complementary R; and iii) the linear degradation of A and W by the exonuclease enzyme. We remind that in PEN reactions certain strands, here R and T_A, are protected against degradation and their concentrations remain constant.

Sequence design allows to make the autocatalysis A slow and non-saturable and its repression by R fast and saturable. Thus, as long as [A] is low enough, the fast repression pathway controls the global kinetics making the concentration of A tend to 0. In return, above a certain threshold, $[A]_{th} \approx [R]$, A will saturate repression and autocatalytic amplification will control the kinetics of the reaction network, bringing [A] to a non-zero steady state balanced by production and degradation. We conclude that such network is bistable (i.e. it has only two possible outcomes for all possible initial concentrations of A) and [R] is a bifurcation parameter of the bistable network because it sets the threshold $[A]_{th}$.

The authors generated a gradient of R in a 5 cm-long glass capillary of rectangular cross-section while the concentrations of all other species (A, T_A, dNTPs and enzymes) were uniform (Figure 1.5g). In these conditions, A grew autocatalytically on the left side of the channel, where [R] is low. This created a front profile of [A] that propagated from left to right through a reaction-diffusion process [153], until it reached the bifurcation concentration of R. At this point the propagation of the front stoped reaching a steady-state, creating

two chemically-distinct zones (presence of A, absence of A).

By assembling two bistables one obtains a tetrastable network with two autocatalytic nodes A and B and a strand R_A-R_B that represses both (Figure 1.5f). In the presence of a gradient of R_A-R_B, such system produces a French flag pattern inside a channel reactor. As expected, this pattern is made of three chemically distinct zones separated by sharp borders: on the left side species A and B are produced, in the center, only A is produced, and on the right side, neither A nor B are produced (Figure 1.5h). Importantly, the pattern was stable for several hours.

In order to mimic material differentiation during embryo development, DNA-coated beads were used. A channel containing a uniform suspension of beads that could be aggregated with either strand A or B produced a 3-band pattern of aggregated beads that superimposed with the 3-band pattern of DNA concentration (Figure 1.5h).

Recently, the lifetime of PEN reactions has been significantly increased [132], generating positional information patterns that lasted more than 60 hours inside millimetric tangible pieces of hydrogel immersed in oil [131]. The compatibility of PEN pattern formation with materials such as beads and hydrogels is an important feature to develop materials inspired from embryo development.

1.3.3.3. Transcription-translation patterns

Gene regulation is used by living organisms to build out-of-equilibrium chemical behaviors that allow them to adapt to a changing environment and process chemical information. During gene regulation, a gene G_A is transcribed by an RNA polymerase into RNA R_A, which is subsequently translated by the ribo-

some into protein P_A. It may happen that P_A has the property of regulating gene production, either from a different gene G_i or from itself. For instance, by blocking or promoting the transcription reaction, thus causing respectively the repression or the activation of the downstream protein. In that case, P_A is called a transcription factor. This way, using transcription and translation reactions, regulatory networks can be constructed.

Since the 1960s, it is possible to recapitulate these reactions outside of living cells using so-called cell-free transcription-translation (TX-TL) systems [31]. In the last two decades, the purity and performances of the cell-free TX-TL systems have been greatly enhanced. For example, improving chemical energy regeneration pathways allows keeping gene regulatory networks out-of-equilibrium inside open reactors [96, 54]. These efforts have also permitted to use TX-TL networks to study pattern formation.

Isalan, Lemerle and Serrano published in 2005 a seminal paper demonstrating that positional information patterns could be obtained using cell-free TX-TL reactions [48]. The experimental setup was crude but allowed to implement a spatial bistability mechanism and produce patterns related to those observed in the *Drosophila* gap gene network discussed above.

More recently, Karzbrun, Bar-Ziv and collaborators introduced an open microfluidic spatial reactor where TX-TL reaction networks could be maintained out of equilibrium for long periods of time without perturbing reaction-diffusion dynamics [54]. Using this device they implemented positional information over a system of diffusively-coupled genetic oscillators [123] (Figure 1.5, bottom panel). The oscillator is encoded through a nonlinear activator-repressor loop of transcription factors. $\sigma 28$ activates the synthesis of CI, which represses $\sigma 28$, forming a loop (Figure 1.5i). Oscillations, i.e. real-time changes in protein con-

centration, are reported by putting the synthesis of green fluorescent protein (GFP) under the control of CI.

To keep the system out of equilibrium the authors used an open reactor composed of diffusively-coupled microchambers (Figure 1.5j). The DNA molecules carrying the corresponding genes are attached to the surface of the microchambers. The chambers are connected to each other through thin channels where gene products can diffuse, forming a one-dimensional array. In addition, each chamber is connected by another thin channel to a wider channel parallel to the array, where a continuous flow of all the components necessary for transcription and translation is maintained. This second set of thin channels allows exchange of enzymes and small molecules from and to the wider channel but precludes hydrodynamic flow, and acts as a physical sink, thus keeping the system out of equilibrium.

The authors investigated the reaction-diffusion dynamics of the oscillators. In the absence of a gradient of positional information, the oscillations in each chamber were synchronized if the coupling between the chambers —controlled by channel geometry— was sufficiently strong. In the presence of an underlying gradient of activator gene, spread out over 10 compartments, the synchrony of the oscillators vanished into more complex spatio-temporal patterns (Figure 1.5k). Surprisingly, their oscillating period remained nearly constant, and neighboring compartments could exhibit anti-correlated patterns.

In conclusion, diverse molecular systems have been used to produce patterns of positional information. These systems have now passed their early stages, and are becoming increasingly complex. All of these methods rely on DNA molecules and thus convert molecular information into spatial complexity. They start to be mature to be coupled to materials and implement the

idea of ‘genome for a material’.

1.4. Force generation and morphogenesis in reconstituted cytoskeletal active gels

As outlined in the introduction, the basics of morphogenesis are anisotropic mechanical forces generated under the control of chemical species. In the living embryo, mechanical forces are largely exerted by the cytoskeleton, which is a complex set of protein filaments and molecular motors that hydrolyze ATP and generate local forces. In this section, we will review materials made of reconstituted cytoskeletal gels that induce macroscopic forces and deformations in vitro. We start by summarizing the basic properties of cytoskeletal proteins. We then briefly introduce the hydrodynamic theory of active gels to help the reader understand the mechanisms underlying active gel contractions. Finally, we review the panoply of structures and shapes that can be generated by cytoskeletal proteins in vitro: gliding filaments, aster formation, contractions, active flows, corrugations and vesicle and droplet deformations.

1.4.1. Cytoskeletal filaments and molecular motors, the building blocks of active gels

The cytoskeleton plays a central role in the organization of eukaryote cells. It is a dynamic structure and a prototypical dissipative material that has been investigated both for its fundamental importance in biology [20, 10] and as a building block of artificial systems [94, 1]. Two of the main constituents of the cytoskeleton are actin filaments and microtubules and their associated

molecular motors.

These two filamentous systems have very different physico-chemical properties associated with distinct cellular functions. Actin filaments are polymers of actin with a double-helical structure that make them relatively flexible (with a persistence length $l_p \approx 20$ μm [11, 1]). Microtubules are polymers of tubulin with a tubular structure that make them particularly rigid ($l_p \approx 1 - 5$ mm) but allow them to buckle when compressed [116, 1]. Both types of filaments are polar, with a minus and a plus end, and both polymerization and depolymerization rates are significantly biased by polarity. Polymerization consumes energy (from ATP in the case of actin [10] and from GTP for microtubules [85]) while depolymerization may happen spontaneously [85, 13]. However, filament length may be stabilized by using drugs, such as taxol for microtubules and phalloidin for actin filaments. In vitro, these filaments may form homogeneous solutions and liquid crystals, respectively at low and high monomer concentration [41], bundles of filaments in the presence of crowding agents [95], branched networks in the presence of branching proteins [10, 124], or crosslinked gels with the help of cross-linking proteins [10].

Myosins, kinesins and dyneins are the families of motors that move along cytoskeletal filaments and exert forces by hydrolyzing ATP. They are essentially composed of two parts: a globular head domain that binds to the filament, hydrolizes ATP and generates forces, and a filamentous tail domain that transfers the force to other cellular structures, in particular to other motors to generate material deformations or to cargos that need to be transported within the cytoplasm. Myosins move along actin filaments and kinesins [133] and dyneins do so along microtubules. In every organism there are tens of different types of these motors with different characteristics [134, 10]. Except

for rare cases, motors move specifically towards one end of the polar filament: most myosins and kinesins move towards the plus-end whereas most dyneins move towards the minus-end of their respective filaments. Typically, myosin motors are weakly processive and form multi-motor complexes in vivo. On the other hand, kinesins are processive and they are found as single motors in vivo. In addition, actomyosin complexes generate forces that make cells deform and move —with an important role during embryo morphogenesis— and microtubules and kinesins and dyneins deal with intracellular transport —in particular during cell division.

1.4.2. Active gel theory for a 1D system

Active gels are materials with the rheological properties of a gel that are able to convert chemical energy into macroscopic forces. The combination of (i) cytoskeletal molecular motors (ii) polar filaments, and (iii) filament cross-linkers is the minimal system to make an active gel in the presence of ATP. A high concentration of ATP and of molecular motors will induce a displacement of the filaments and set the gel in motion.

One way to describe these systems, in which chemical reactions induce forces, is to add chemical terms to the hydrodynamic equations that describe the deformation of a gel. To obtain the expression of these *chemical forces* we follow the approach developed by Onsager in 1931, and applied to active gels by Kruse, Sekimoto and coworkers [62], to determine the *fluxes* and the corresponding conjugate *forces* that govern the out-of-equilibrium evolution of the gel [97]. In Onsager's vocabulary, a thermodynamic force is a quantity whose difference induces a flux between two points. For instance, the temperature is

a force that induces a heat flux. For a system not too far from an equilibrium state, the fluxes can be expressed as linear combinations of the several forces by introducing phenomenological coefficients. This is for example what happens in the Soret effect where a diffusive particle flux is induced by a temperature gradient identified as a thermodynamic force. As an example, we use Onsager's approach to derive the dynamical equations that describe the deformation of a 1D active gel as illustrated in the top panel of Figure 1.6.

The reactive state of the gel is described using the concentrations c_i and the chemical potentials μ_i of the chemical species i, and its mechanical state with the mass density ρ and the velocity field v that describes the gel's motion. The spatial coordinate is noted x. As a first approximation, one may consider solely the reaction ATP $\rightarrow$ ADP+Pi. We will see that this reaction induces a chemical force identified to the difference of chemical potential $\Delta\mu$ of ATP hydrolysis and a flux related to the reaction rate $r = -dc_{ATP}/dt$, while the mechanical deformation of the gel induces a mechanical force given by a velocity gradient dv/dx and a flux given by the stress σ.

We first express the free energy F of the active gel

$$F \;=\; F_{chem} + F_{kin} \tag{1.15}$$

that is the sum of its chemical free energy F_{chem}, which for reactions in solution can be approximated with the chemical free enthalpy $G_{chem} = \int dx(\mu_{\mathrm{ATP}}c_{\mathrm{ATP}} + \mu_{\mathrm{ADP}}c_{\mathrm{ADP}} + \mu_{\mathrm{Pi}}c_{\mathrm{Pi}})$, and the kinetic energy of the gel, $F_{kin} = \int dx \left(\frac{1}{2}\rho v^2\right)$. The free energy can be written as $F = U - TS$, with U the internal energy, T the temperature and S the entropy. During the non-equilibrium process that we are trying to describe, the rate of change dF/dt can be written as the sum of a reversible part $dF_{rev}/dt = dU/dt$, that we assume to vanish here as no work or

external forces are considered, and an irreversible part $dF_{irr}/dt = -TdS/dt$. Using the conservation laws for chemical species, for the mass and for the momentum of the gel, we derive the irreversible part of the free energy rate that can be written as

$$\begin{aligned} T\frac{dS}{dt} &= -\frac{dF}{dt} \\ &= -\int dx \left(r\Delta_r G + \sigma \frac{dv}{dx} \right) , \end{aligned} \tag{1.16}$$

where $r = -dc_{\mathrm{ATP}}/dt$ is the rate of ATP consumption and $\Delta_r G = \mu_{\mathrm{ATP}} - \mu_{\mathrm{ADP}} - \mu_P$ is the free enthalpy of ATP hydrolysis. σ is the 1D tension of the active gel, also identified as the momentum flux in the gel. Its spatial derivative $d\sigma/dx$ is the local force.

The entropy production rate is the sum of two dissipative terms that can each be decomposed into a *flux* and a thermodynamic *force*: (i) a chemical contribution $r\Delta_r G$, where the free enthalpy of the ATP hydrolysis, $\Delta_r G$, and the reaction rate, r, are identified as the chemical thermodynamic force and the associated flux, respectively, and (ii) a mechanical contribution $\sigma \frac{dv}{dx}$, where the velocity gradient dv/dx and the 1D tension σ can be identified as conjugate forces and fluxes.

Assuming that the system evolves close to an equilibrium state, the fluxes (σ, r) can be expressed as linear functions of the forces (dv/dx, $\Delta_r G$). Introducing Onsager coefficients η, ζ and Λ, one gets

$$\sigma = \eta \frac{dv}{dx} + \zeta \Delta_r G \, , \tag{1.17}$$

$$r = \Lambda \Delta_r G - \zeta \frac{dv}{dx} \, , \tag{1.18}$$

where η can be identified as the 1D viscosity of the gel. The coefficient Λ is equal to the rate constant of ATP hydrolysis rescaled by k_bT. Finally, the proportionality coefficient between the chemical force $\Delta_r G$ and the mechanical flux σ, and between the chemical flux r and the mechanical force dv/dx, ζ, is identical due to Onsager reciprocal relations

The first equation illustrates the chemo-mechanical coupling present in these systems at the macroscopic scale. The stress σ is the sum of a passive viscous term $\eta dv/dx$ and an active term $\zeta\Delta_r G$ proportional to the free enthalpy of ATP hydrolysis. The second equation illustrates that these systems present also a mechano-chemical coupling, the rate of hydrolysis depending on the velocity gradient of the flow within the gel. As the active gel theory has been developed by physicists with the goal of describing the shape change of active gels, the first equation has been largely studied for systems of increasing complexity [79]. The second equation, on the contrary, is rarely considered.

To illustrate the contraction of an active gel, for which we will provide experimental examples below, we apply equation (1.17) to the deformation of a 1D active gel of length L under a constant active tension $\zeta\Delta_r G$ induced by molecular motors (Figure 1.6c). The active forces are offset by external forces applied at the edges. At $t = 0$, the external forces and the stresses at the boundaries vanish and the gel contracts under active tension. In these systems, inertia can be neglected and thus the equilibrium of forces must be met at every point, which is written $\partial_x \sigma = 0$. This equation combined with (1.17) yields

$$0 \;=\; \eta \frac{d^2 v}{dx^2} + \frac{d\zeta\Delta_r G}{dx}\,. \tag{1.19}$$

As the active tension is uniform, the last term vanishes and we have $0 = \eta\frac{d^2 v}{dx^2}$. Integrating this last equation, we find that the initial velocity of the gel material

is equal to $v = -\frac{\zeta \Delta_r G}{\eta} x$ and corresponds to a contraction of the gel.

The theory of active gels can also take into account the polarity of the filaments by incorporating concepts from the hydrodynamic theory of liquid crystals [63, 52]. This powerful theory accounts for the majority of the observations described in the next sections. In addition, it has been successfully applied to active gels in living systems [16, 35, 72, 90].

1.4.3. Active structures generated by cytoskeletal systems in vitro

In the following, we will describe various motile and non-motile structures that can be generated in vitro by combining cytoskeletal motors and filaments in different ways. Importantly, all these structures are out-of-equilibrium and need ATP or GTP hydrolysis to be created and sustained —primarily through motor activity.

1.4.3.1. Gliding filaments

The most straightforward approach to observe macroscopic movement in mixtures of filaments and motors is the gliding assay. In these experiments, motors are adsorbed on a surface and filaments move parallely to the surface plane entrained by the motors in the presence of ATP [135, 61]. When the concentration of the filaments increases, collective motion is observed. Examples are density waves of actin filaments on myosin carpets [111] (Figure 1.6d) and vortices of microtubules on dynein [118] and kinesin [47] layers. Importantly, the formation of these microtubule vortices has recently been controlled with DNA by using DNA-tubulin chimeras [57].

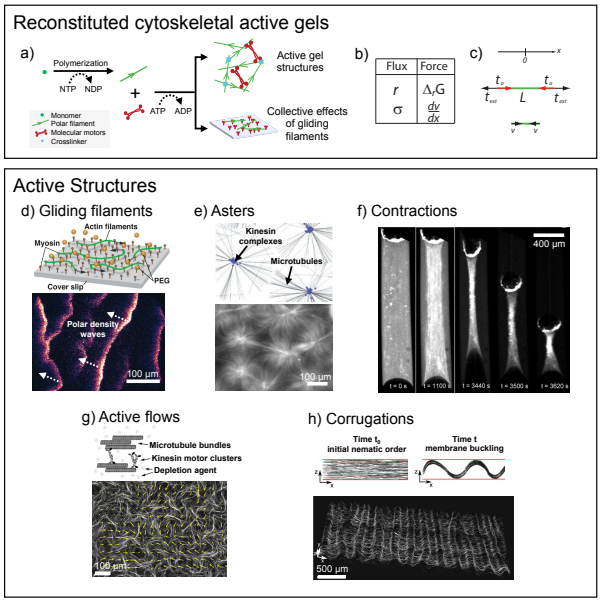

Figure 1.6: Force generation and morphogenesis in reconstituted cytoskeletal active gels. a) These gels are made of polymerized filaments, molecular motors and, potentially, passive crosslinkers, see text. In the presence of a source of energy (GTP and/or ATP), active gels form complex out-of-equilibrium 3D structures or lead to 2D collective effects. b) Pairs of conjugate thermodynamic fluxes and forces in active gels. c) Modelisation of a contracting 1D active gel. d) Polar patterns of actin filaments driven by adsorbed myosin motors. At high concentration of filaments, density waves are observed. Adapted from [45]. e) Self-organization of microtubules and motors into a lattice of asters. The structures are polarity-sorted with an accumulation of motors in the center. Adapted from [119] and [93]. f) Timelapse of a contractile actin-myosin-α actinin gel. Adapted from [8], with permission from the Biophysical Society. g) Internally-driven, chaotic flows of microtubule bundles formed by depletion forces and kinesin clusters. Adapted from [109]. h) A 3D active nematic fluid creates a stable corrugated sheet of well-defined wavelength [113].

1.4.3.2. Aster formation

When aggregates of motors are mixed with filaments at low motor/filament ratios in a solution containing ATP, star-shaped structures of radially-oriented filaments appear spontaneously. These structures, called asters, were first observed by Nédélec, Surrey and co-workers using kinesin-1 aggregates mixed

with static microtubules stabilized with taxol (Figure 1.6e) [93]. Kinesin aggregates were obtained with biotinylated kinesin coupled to streptavidin as an artificial mimic of natural microtubule-crosslinking motors such as kinesin-5 [20]. Importantly, asters are polar structures, with filament plus-ends at the center and minus-ends at the periphery when plus-end kinesin aggregates were used [119]. Computer simulations suggest that aster formation is due to the accumulation of motors at the microtubule plus-ends [119]. Asters have also recently been observed in dynein/microtubule [122] and myosin-2/actin filament systems [145].

1.4.3.3. Contractions

When motor aggregates are mixed with filaments at higher motor/filament ratios than for asters, a global contraction of the 3-dimensional meshwork made of filaments and motors is observed. Global contraction was first reported by Szent-György in 1942 in actomyosin gels from cell extracts [94]. More recently, actomyosin contractions have been quantified in purified solutions containing actin filaments, myosin II motor aggregates, and α-actinin cross-linkers [8]. Typically, 10 μL of this active gel contracted to 5% of its volume within 30 min, exerting forces of $\sim$ 1 μN (Figure 1.6f). Contractions were observed at sufficiently high myosin/actin ratios and at intermediate cross-linker/actin ratios [8]. So far, it has not been possible in vitro to restart a collapsed actin network. In contrast, in vivo, actomyosin induces highly dynamic behaviors due to the rapid renewal of actin filaments [89, 84]. Global contractions of microtubule networks have been observed in egg extracts [28], where they were suggested to arise from dynein aggregates, and in purified microtubule gels [126] in the presence of kinesin-5, which is a motor with two heads that pulls

on two filaments at once.

1.4.3.4. Active flows

Aster formation needs the accumulation of motor aggregates on one end of the filament extremities. Suppressing motor accumulation should make filaments continuously slide along each other, creating filament flows that may induce macroscopic flows in the solution. This is of particular interest to physicists because it is a novel way of inducing liquid flow without applying an external pressure [141, 79]. This fascinating behavior was first observed by Sanchez, Dogic and collaborators [108] by simply adding a depletion agent (a hydrophilic polymer) to a solution of kinesin aggregates and microtubules that otherwise would produce asters (Figure 1.6g). Depletion forces induce a net attraction between microtubules that aggregate into bundles [95, 12]. These bundles contain filaments oriented in both plus and minus directions and are thus weakly polar. As a result, motor aggregates will no more accumulate preferentially at one end of the bundle and these will incessantly slide along each other carried away by motors. Passive brownian particles immersed in such a solution were entrained by the active flow of bundles with velocities up to 2 μm/s, demonstrating the generation of macroscopic fluid flows. These flows where chaotic, with vortices of typically 100 μm, but could be rectified in a toroidal geometry, generating coherent flows that allowed the macroscopic transport of liquid along circuits up to one meter long [148], confirming previous theoretical predictions [141].

In a recent study, Roostalu and collaborators [106] introduced a different way to suppress motor accumulation at filament ends: use dynamic filaments that grow at the extremity where the motors would tend to accumulate. In this

situation, chaotic flows were observed in the absence of a depletion agent. In addition, the authors demonstrated that the same system could form asters, contract, or display chaotic flows, depending on the control parameters. Higher filament concentrations and growth rates promoted chaotic flows, while low concentrations and growth rates favored aster formation. In addition, increasing motor and filament concentrations promoted global contractions.

Interestingly, these 3D active flows can also be observed in 2D by just putting the active solution in the presence of a water/oil interface. In this situation, the depletion agent not only creates filament bundles but also pushes them to the interface [108]. This forms a 2D liquid crystal nematic phase at the interface, creating a new type of soft material: an active nematic liquid crystal. In particular, the defects that inevitably appear in the nematic phase, display rich dynamics [108, 21, 81, 98]. Although all these observations were initially made in microtubule/kinesin systems, active nematic phases have been recently reported in actin/myosin systems as well [64]. Interestingly, all these striking non-equilibrium behaviors can be maintained in a closed-reactor for several hours.

1.4.3.5. Corrugations

In 1990 Tabony and Job demonstrated that a solution of tubulin that polymerizes into microtubules by consuming GTP self-organizes into a stripe pattern [120]. Initially interpreted as arising from a reaction-diffusion mechanism [33], it is now clear that these patterns result from local forces exerted by growing filaments [73]. These patterns were obtained in a channel reactor of rectangular cross-section that was long in the x direction and thin in z. The boundaries forced the initially short filaments to be aligned along the long axis of the

channel. Upon growth, the filaments pushed each other producing periodic corrugations in the xy plane.

More recently, Senoussi et al. demonstrated that a different type of corrugations could be observed with active gels that are prone to producing chaotic flows [113] (Figure 1.6h). The authors introduced, in a channel of rectangular cross-section, a solution of kinesin aggregates and microtubule bundles in the presence of a depletion agent and ATP. In this study, the microtubules were significantly longer than those used in the chaotic flow experiments described above (10 *vs.* 2 μm, respectively). As a result, during the loading of the channel, the filament bundles orientate parallely to the x axis and form a nematic phase. Passive forces due to depletion induced this solution to form a thin nematic sheet that buckled in the xz plane due to active extensile forces and generated a centimeter-sized periodic corrugated pattern with a typical wavelength of 100 μm. The wavelength could be tuned by the active forces —the motor concentration— or by the bending modulus of the sheet —for example, the thickness of the gel. At high motor concentration the pattern was only transient and ultimately broke into the chaotic flow state described earlier.

Active buckling has also been reported in contractile poroelastic actomyosin sheets [46]. A crosslinked network of actin is contracting because of the presence of aggregates of myosin motors, and buckles at its edges.

These three examples illustrate how cytoskeletal active gels can be used to engineer morphogenesis in a macroscopic non-living material.

1.4.3.6. Vesicle and droplet deformation and movement

The encapsulation of cytoskeletal active gels inside water-in-water vesicles or water-in-oil droplets is an attractive strategy to either deform or induce move-

ment to a soft material, a topic that has been recently reviewed [6]. The deformation of vesicles containing growing microtubules or polymerizing actin in the absence of motors was demonstrated in the early 1990s by Hotani and coworkers [43, 86]. Polymerizing microtubules initially deform the vesicle into a rugby-ball shape with thin tubes later emerging from each pole [43, 30, 25, 102], while actin formed dumbbell-shaped vesicles [86]. Crosslinked actin and actomyosin gels were later encapsulated inside vesicles, which induced a variety of gel structures but without modifying the shape of the vesicle: actin rings, webs [70] and cortices [103], 3D gels [121, 127] and contracting cortices [18]. Vesicle deformation induced by actomyosin dynamics was demonstrated more recently [74]. In addition, in an experimental tour de force, Sato and collaborators engineered a vesicle containing microtubules and kinesins coupled to the vesicle's membrane through DNA hybridization and were able to induce DNA-controlled periodic membrane deformations [110]. In a different context, the Min oscillatory system described earlier (section 1.2.4), was recently reported to induce vesicle shape deformation, possibly by the transient recruitement of protein MinE on the membrane [71, 34].

The encapsulation of microtubule bundles and kinesin aggregates (see above) inside droplets generated 2D flows close to the membrane interface that resulted in droplet movement [108]. These active nematic droplets submerged in an oil that naturally presents a liquid crystalline structure, produced a strong coupling in the dynamics of defects between the active and the passive liquid crystal [38]. Inside liposomes, the forces exerted by the active nematic distorted the spherical shape of the liposome and generated sharp appendixes [56, 159]. In addition, polymerizing microtubules in the presence of kinesin aggregates produced cortical bundles [7] and asters [7, 53], structures that were greatly

influenced by the membrane composition [53]. Finally, Weirich et al. recently reported that membraneless actomyosin droplets were able to form and divide inside an aqueous solution [144].

In summary, active cytoskeletal systems display in vitro a variety of dynamic behaviors that are characterized by two features: the generation of local forces by motors —or polymerizing filaments— that consume chemical energy, and the properties of the composite material where these forces are exerted —a liquid crystal or a cross-linked gel, for instance. These behaviors, that can be described using the hydrodynamic theory of active gels, result in pattern formation, such as asters, in the motion of macroscopic objects, such as droplets, or in their deformation, as we have seen for active corrugations. In the future, coupling the pattern formation systems discussed previously with active gel deformations appears as a promising strategy for obtaining out-of-equilibrium materials that emulate essential aspects of embryo development.

1.5. Conclusion and perspectives

We have attempted to illustrate that embryo development is a useful source of inspiration to design and synthesize non-equilibrium materials. In this context, we have considered embryo development as a molecular self-construction process that transforms an amorphous mass into a highly differentiated material. This multistep process occurs by interpreting chemical information through a non-equilibrium process that consumes chemical energy. The successful implementation of this idea would provide artificial soft materials that build themselves following a developmental program, which may have applications for material fabrication in remote locations —in space or inside a living organism—

or when massive parallelism is needed.

We have focused our attention on two critical steps of the embryo development: pattern formation and morphogenesis. Although both phases involve molecular interactions, we argued that the former is essentially a chemical process while the latter is mechanical. We have demonstrated that developmental pattern formation is generally accounted for by two fundamental mechanisms: Turing patterns and positional information. The Turing model is theoretically attractive; however, it imposes severe constraints on the reaction mechanism. Hence, the positional information model has been widely employed. For example, this concept is at play in the formation of anteroposterior patterns of protein concentration in the early development of the fruit fly. Additionally, positional information patterns have recently been successfully implemented in vitro with three different rational approaches: DNA hybridization, PEN DNA/enzyme and transcription-translation reactions. We believe that these approaches are now mature to explore the coupling between chemical and morphological differentiation.

The implementation of chemo-mechanical coupling, which is essential for morphogenesis, has been a long quest in chemistry. In this regard, our review is far from being exhaustive. We have focused on reconstituted gels of cytoskeletal proteins, which take advantage of powerful biological motors and display a rich variety of dynamical behaviors; from force-induced pattern formation to movement and deformation of macroscopic soft materials. For reasons of space we have not mentioned the use of synthetic molecular motors [55], of which Feringa provides a review in an accompanying chapter of this book, and that have recently been coupled to shape changes of macroscopic materials [69]. Other possibilities are illustrated by hydrogel deformation [82], in particular

when coupled to the Belousov-Zhabotinsky oscillator [151, 150] or to DNA concentrations [17], by microfabricated homeostatic materials [40] and by osmotic forces in droplet assemblies [140]. In addition to active cytoskeleton gels, all these systems could be utilized to accomplish chemo-mechanical coupling in the perspective explored here.

The coupling of pattern formation to morphogenesis is, in our opinion, an important next step in our quest to build materials inspired from embryogenesis. This coupling is common in natural systems, such as the developing embryo, but is unknown in synthetic materials. This knowledge is vital for the advanced programming of self-organizing macroscale shapes at the molecular level. The systems discussed in this chapter could all be used to reach this goal in a near future. The development of such materials will undoubtedly lead to so far elusive self-fabricated, force-exerting synthetic soft matter with the potential of integration in soft robotics and biological environments.

1.6. Acknowledgment

We thank Yannick Rondelez, Anton Zadorin, Georg Urtel, Guillaume Gines, Anthony Genot, Ananyo Maitra, Raphael Voituriez and Thomas Surrey for valuable discussions and Guillaume Sarfati for a careful reading of the manuscript. This research has been supported by CNRS (H.B, J.-C.G. and A.E.-T.), by the European Research Council (ERC) under the European's Union Horizon 2020 programme (grant No 770940, A.E.-T.) and by the Ville de Paris Emergences programme (Morphoart, A.E.-T.).

Bibliography

[1] Rachel Andorfer and Joshua D. Alper. From isolated structures to continuous networks: A categorization of cytoskeleton-based motile engineered biological microstructures. *Wiley Interdisciplinary Reviews: Nanomedicine and Nanobiotechnology*, 11(4): e1553, 2019. ISSN 1939-5116. doi: 10.1002/wnan.1553. URL https://onlinelibrary.wiley.com/doi/abs/10.1002/wnan.1553.

[2] Alexandre Baccouche, Kevin Montagne, Adrien Padirac, Teruo Fujii, and Yannick Rondelez. Dynamic dna-toolbox reaction circuits: A walkthrough. *Methods*, doi:10.1016/j.ymeth.2014.01.015, 2014. ISSN 1046-2023. doi: http://dx.doi.org/10.1016/j.ymeth.2014.01.015. URL http://www.sciencedirect.com/science/article/pii/S1046202314000255.

[3] Philip Ball. Forging patterns and making waves from biology to geology: a commentary on turing (1952) 'the chemical basis of morphogenesis'. *Philosophical Transactions of the Royal Society B: Biological Sciences*, 370, 2015.

[4] T. Bansagi, V. K. Vanag, and I. R. Epstein. Tomography of reaction-diffusion microemulsions reveals three-dimensional turing patterns. *Science*, 331(6022):1309–1312, 2011. ISSN 0036-8075. doi: 10.1126/science.1200815. URL <Go to ISI>://WOS:000288215200042.

[5] T. Bansagi, V. K. Vanag, and I. R. Epstein. Two- and three-dimensional standing waves in a reaction-diffusion system. *Phys. Rev. E*, 86(4), 2012. ISSN 1539-3755. doi: 04520210.1103/PhysRevE.86.045202. URL <Go to ISI>://WOS:000309815000001.

[6] Yashar Bashirzadeh and Allen P. Liu. Encapsulation of the cytoskeleton: towards mimicking the mechanics of a cell. *Soft Matter*, 15(42): 8425–8436, 2019. ISSN 1744-683X. doi: 10.1039/C9SM01669D. URL http://dx.doi.org/10.1039/C9SM01669D.

[7] Hella Baumann and Thomas Surrey. Motor-mediated cortical versus astral microtubule organization in lipid-monolayered droplets. *Journal of Biological Chemistry*, 289(32):22524–22535, 2014. doi: 10.1074/jbc.M114.582015. URL http://www.jbc.org/content/289/32/22524.abstract.

[8] Poul M. Bendix, Gijsje H. Koenderink, Damien Cuvelier, Zvonimir Dogic, Bernard N. Koeleman, William M. Brieher, Christine M. Field, L. Mahadevan, and David A. Weitz. A quantitative analysis of contractility in active cytoskeletal protein networks. *Biophysical journal*, 94(8): 3126–3136, 2008. ISSN 1542-0086 0006-3495. doi: 10.1529/biophysj.107.117960. URL https://www.ncbi.nlm.nih.gov/pubmed/18192374 https://www.ncbi.nlm.nih.gov/pmc/PMC2275689/ https://www.ncbi.nlm.nih.gov/pmc/articles/PMC2275689/pdf/3126.pdf.

[9] J. Craig Blain and Jack W. Szostak. Progress toward synthetic cells. *Annual Review of Biochemistry*, 83(1):615–640, 2014. ISSN 0066-4154. doi: 10.1146/annurev-biochem-080411-124036. URL https://doi.org/10.1146/annurev-biochem-080411-124036.

[10] Laurent Blanchoin, Rajaa Boujemaa-Paterski, Cécile Sykes, and Julie Plastino. Actin dynamics, architecture, and mechanics in cell motility. *Physiological Reviews*, 94(1):235–263, 2018/05/09 2014. doi: 10.1152/physrev.00018.2013. URL https://doi.org/10.1152/physrev.00018.2013.

[11] Clifford P. Brangwynne, Gijsje H. Koenderink, Ed Barry, Zvonimir Dogic, Frederick C. MacKintosh, and David A. Weitz. Bending dynamics of fluctuating biopolymers probed by automated high-resolution filament tracking. *Biophysical Journal*, 93(1):346–359, 2007. ISSN 0006-3495. doi: https://doi.org/10.1529/biophysj.106.096966. URL http://www.sciencedirect.com/science/article/pii/S0006349507712870 https://www.ncbi.nlm.nih.gov/pmc/articles/PMC1914425/pdf/346.pdf.

[12] Marcus Braun, Zdenek Lansky, Feodor Hilitski, Zvonimir Dogic, and Stefan Diez. Entropic forces drive contraction of cytoskeletal networks. *BioEssays*, 38(5):474–481, 2016. doi: doi:10.1002/bies.201500183. URL https://onlinelibrary.wiley.com/doi/abs/10.1002/bies.201500183.

[13] William Brieher. Mechanisms of actin disassembly. *Molecular biology of the cell*, 24(15):2299–2302, 2013. ISSN 1939-4586 1059-1524. doi: 10.1091/mbc.E12-09-0694. URL https://www.ncbi.nlm.nih.gov/pubmed/23900650 https://www.ncbi.nlm.nih.gov/pmc/articles/PMC3727922/. 23900650[pmid] PMC3727922[pmcid] 24/15/2299[PII].

[14] J. Briscoe and S. Small. Morphogen rules: design principles of gradient-mediated embryo patterning. *Development*, 142(23):3996–4009, 2015. ISSN 1477-9129 (Electronic) 0950-1991 (Linking). doi: 10.1242/dev.129452. URL http://www.ncbi.nlm.nih.gov/pubmed/26628090.

[15] Bastiaan C. Buddingh and Jan C. M. van Hest. Artificial cells: Synthetic compartments with life-like functionality and adaptivity. *Accounts of Chemical Research*, 50(4):769–777,

2017. ISSN 0001-4842. doi: 10.1021/acs.accounts.6b00512. URL https://doi.org/10.1021/acs.accounts.6b00512.

[16] A. C. Callan-Jones and R. Voituriez. Active gel model of amoeboid cell motility. *New Journal of Physics*, 15(2):025022, 2013. ISSN 1367-2630. doi: 10.1088/1367-2630/15/2/025022. URL http://dx.doi.org/10.1088/1367-2630/15/2/025022.

[17] Angelo Cangialosi, ChangKyu Yoon, Jiayu Liu, Qi Huang, Jingkai Guo, Thao D. Nguyen, David H. Gracias, and Rebecca Schulman. Dna sequence–directed shape change of photopatterned hydrogels via high-degree swelling. *Science*, 357(6356):1126–1130, 2017.

[18] Kevin Carvalho, Feng-Ching Tsai, Edouard Lees, Raphal Voituriez, Gijsje H. Koenderink, and Cecile Sykes. Cell-sized liposomes reveal how actomyosin cortical tension drives shape change. *Proceedings of the National Academy of Sciences*, 110:16456–16461, 2013.

[19] V. Castets, E. Dulos, J. Boissonade, and P. De Kepper. Experimental evidence of a sustained standing turing-type nonequilibrium chemical pattern. *Phys. Rev. Lett.*, 64(24):2953, 1990. URL http://link.aps.org/doi/10.1103/PhysRevLett.64.2953.

[20] Marileen Dogterom and Thomas Surrey. Microtubule organization in vitro. *Current Opinion in Cell Biology*, 25 (1):23–29, 2013. doi: 10.1016/j.ceb.2012.12.002. URL http://www.sciencedirect.com/science/article/pii/S0955067412001925.

[21] Amin Doostmohammadi, Jordi Ignés-Mullol, Julia M. Yeomans, and Francesc Sagués. Active nematics. *Nature Communications*, 9(1):

3246, 2018. ISSN 2041-1723. doi: 10.1038/s41467-018-05666-8. URL https://doi.org/10.1038/s41467-018-05666-8.

[22] W Driever and C Nüsslein-Volhard. The bicoid protein determines position in the drosophila embryo in a concentration-dependent manner. *Cell*, 54:95–104, 1988.

[23] Wolfgang Driever and Christiane Nüsslein-Volhard. A gradient of bicoid protein in drosophila embryos. *Cell*, 54(1):83–93, 1988.

[24] Andrew D. Economou, Atsushi Ohazama, Thantrira Porntaveetus, Paul T. Sharpe, Shigeru Kondo, M. Albert Basson, Amel Gritli-Linde, Martyn T. Cobourne, and Jeremy B. A. Green. Periodic stripe formation by a turing mechanism operating at growth zones in the mammalian palate. *Nat. Genet.*, 44(3):348–351, 2012. ISSN 1061-4036. doi: 10.1038/ng.1090. URL http://dx.doi.org/10.1038/ng.1090. 10.1038/ng.1090.

[25] Virginie Emsellem, Olivier Cardoso, and Patrick Tabeling. Vesicle deformation by microtubules: A phase diagram. *Physical Review E*, 58(4):4807–4810, 1998. doi: 10.1103/PhysRevE.58.4807. URL https://link.aps.org/doi/10.1103/PhysRevE.58.4807 https://journals.aps.org/pre/pdf/10.1103/PhysRevE.58.4807. PRE.

[26] I. Epstein and J. A. Pojman. *An introduction to nonlinear chemical reactions*. Oxford University Press, New York, 1998.

[27] Irving R. Epstein and Bing Xu. Reaction-diffusion processes at the nano-

and microscales. *Nat Nano*, 11(4):312–319, April 2016. ISSN 1748-3387. URL http://dx.doi.org/10.1038/nnano.2016.41.

[28] Peter J. Foster, Sebastian Fürthauer, Michael J. Shelley, and Daniel J. Needleman. Active contraction of microtubule networks. *eLife*, 4: e10837, 2015. ISSN 2050-084X. doi: 10.7554/eLife.10837. URL https://doi.org/10.7554/eLife.10837.

[29] Teruo Fujii and Yannick Rondelez. Predator-prey molecular ecosystems. *ACS Nano*, 7(1):27–34, 2013.

[30] Deborah Kuchnir Fygenson, John F. Marko, and Albert Libchaber. Mechanics of microtubule-based membrane extension. *Physical Review Letters*, 79(22):4497–4500, 1997. doi: 10.1103/PhysRevLett.79.4497. URL https://link.aps.org/doi/10.1103/PhysRevLett.79.4497. PRL.

[31] David Garenne and Vincent Noireaux. Cell-free transcriptiontranslation: engineering biology from the nanometer to the millimeter scale. *Current Opinion in Biotechnology*, 58:19–27, 2019. ISSN 0958-1669. doi: https://doi.org/10.1016/j.copbio.2018.10.007. URL http://www.sciencedirect.com/science/article/pii/S0958166918300995.

[32] A. Gierer and H. Meinhardt. A theory of biological pattern formation. *Kybernetik*, 12:30–39, 1972. doi: 10.1007/BF00289234.

[33] Nicolas Glade, Jacques Demongeot, and James Tabony. Microtubule self-organisation by reaction-diffusion processes causes collective transport and organisation of cellular particles. *BMC cell biology*, 5:23–23, 2004. ISSN 1471-2121. doi: 10.1186/1471-2121-5-23. URL https://www.ncbi.nlm.nih.gov/pubmed/15176973

https://www.ncbi.nlm.nih.gov/pmc/articles/PMC428571/.
15176973[pmid] PMC428571[pmcid] 1471-2121-5-23[PII].

[34] Elisa Godino, Jons Noguera Lpez, David Foschepoth, Céline Cleij, Anne Doerr, Clara Ferrer Castell, and Christophe Danelon. De novo synthesized min proteins drive oscillatory liposome deformation and regulate ftsa-ftsz cytoskeletal patterns. *Nature Communications*, 10(1): 4969, 2019. ISSN 2041-1723. doi: 10.1038/s41467-019-12932-w. URL https://doi.org/10.1038/s41467-019-12932-w.

[35] Nathan W. Goehring, Philipp Khuc Trong, Justin S. Bois, Debanjan Chowdhury, Ernesto M. Nicola, Anthony A. Hyman, and Stephan W. Grill. Polarization of par proteins by advective triggering of a pattern-forming system. *Science*, 2011. URL http://science.sciencemag.org/content/early/2011/10/27/science.1208619.abstra

[36] J. B. Green and J. Sharpe. Positional information and reaction-diffusion: two big ideas in developmental biology combine. *Development*, 142(7): 1203–11, 2015.

[37] T. Gregor, H. G. Garcia, and S. C. Little. The embryo as a laboratory: quantifying transcription in drosophila. *Trends Genet.*, 30(8):364–75, 2014. ISSN 0168-9525 (Print) 0168-9525 (Linking). doi: 10.1016/j.tig.2014.06.002. URL http://www.ncbi.nlm.nih.gov/pubmed/25005921.

[38] Pau Guillamat, Ziga Kos, Jürme Hardoüin, Jordi Ignés-Mullol, Miha Ravnik, and Francesc Sagués. Active nematic emulsions. *Science Advances*, 4, 2018.

[39] J. Halatek, F. Brauns, and E. Frey. Self-organization principles of intra-

cellular pattern formation. *Phil. Trans. Roy. Soc. B*, 373, 2018. URL http://rstb.royalsocietypublishing.org/content/373/1747/20170107.abstract.

[40] Ximin He, Michael Aizenberg, Olga Kuksenok, Lauren D. Zarzar, Ankita Shastri, Anna C. Balazs, and Joanna Aizenberg. Synthetic homeostatic materials with chemo-mechano-chemical self-regulation. *Nature*, 487(7406):214–218, 2012. ISSN 0028-0836. doi: 10.1038/nature11223. URL http://dx.doi.org/10.1038/nature11223.

[41] A. L. Hitt, A. R. Cross, and R. C. Williams. Microtubule solutions display nematic liquid crystalline structure. *Journal of Biological Chemistry*, 265(3):1639–47, 1990. URL http://www.jbc.org/content/265/3/1639.abstract.

[42] Judit Horvath, Istvan Szalai, and Patrick De Kepper. An experimental design method leading to chemical turing patterns. *Science*, 324(5928):772–775, 2009. URL http://www.sciencemag.org/content/324/5928/772.abstract. 10.1126/science.1169973.

[43] Hirokazu Hotani and Hiroshi Miyamoto. Dynamic features of microtubules as visualized by dark-field microscopy. *Advances in Biophysics*, 26:135–156, 1990. ISSN 0065-227X. URL http://www.sciencedirect.com/science/article/pii/0065227X9090010Q.

[44] Kerwyn Casey Huang, Yigal Meir, and Ned S. Wingreen. Dynamic structures in ¡em¿escherichia coli¡/em¿: Spontaneous formation of mine rings and mind polar zones. *Proceedings of the National Academy of Sciences*, 100:12724–12728, 2003.

[45] L. Huber, R. Suzuki, T. Krüger, E. Frey, and A. R. Bausch. Emergence of coexisting ordered states in active matter systems. *Science*, 361:255–258, 2018.

[46] Y. Ideses, V. Erukhimovitch, R. Brand, D. Jourdain, J. Salmeron Hernandez, U. R. Gabinet, S. A. Safran, K. Kruse, and A. Bernheim-Groswasser. Spontaneous buckling of contractile poroelastic actomyosin sheets. *Nature Communications*, 9(1):2461, 2018. ISSN 2041-1723.

[47] Daisuke Inoue, Bulbul Mahmot, Arif Md Rashedul Kabir, Tamanna Ishrat Farhana, Kiyotaka Tokuraku, Kazuki Sada, Akihiko Konagaya, and Akira Kakugo. Depletion force induced collective motion of microtubules driven by kinesin. *Nanoscale*, 7(43):18054–18061, 2015. ISSN 2040-3364. doi: 10.1039/C5NR02213D. URL `http://dx.doi.org/10.1039/C5NR02213D`.

[48] M. Isalan, C. Lemerle, and L. Serrano. Engineering gene networks to emulate drosophila embryonic pattern formation. *PLoS Biol.*, 3(3):488–496, 2005.

[49] J. Jaeger. Modelling the drosophila embryo. *Mol. Biosyst.*, 5(12):1549–68, 2009. ISSN 1742-2051 (Electronic) 1742-2051 (Linking). doi: 10.1039/b904722k. URL `http://www.ncbi.nlm.nih.gov/pubmed/20023719`.

[50] J. Jaeger, Manu, and J. Reinitz. Drosophila blastoderm patterning. *Curr. Opin. Genet. Dev.*, 22(6):533–41, 2012. ISSN 1879-0380 (Electronic) 0959-437X (Linking). doi: 10.1016/j.gde.2012.10.005. URL `http://www.ncbi.nlm.nih.gov/pubmed/23290311`.

[51] Johannes Jaeger, Svetlana Surkova, Maxim Blagov, Hilde Janssens,

David Kosman, Konstantin N. Kozlov, Manu, Ekaterina Myasnikova, Carlos E. Vanario-Alonso, Maria Samsonova, David H. Sharp, and John Reinitz. Dynamic control of positional information in the early drosophila embryo. *Nature*, 430(6997):368–371, 2004. ISSN 0028-0836. doi: 10.1038/nature02678. URL http://dx.doi.org/10.1038/nature02678.

[52] J. F. Joanny, F. Jülicher, K. Kruse, and J. Prost. Hydrodynamic theory for multi-component active polar gels. *New Journal of Physics*, 9(11): 422–422, 2007. ISSN 1367-2630. doi: 10.1088/1367-2630/9/11/422. URL http://dx.doi.org/10.1088/1367-2630/9/11/422.

[53] Michael P. N. Juniper, Marian Weiss, Ilia Platzman, Joachim P. Spatz, and Thomas Surrey. Spherical network contraction forms microtubule asters in confinement. *Soft Matter*, 14(6):901–909, 2018. ISSN 1744-683X. doi: 10.1039/C7SM01718A. URL http://dx.doi.org/10.1039/C7SM01718A.

[54] Eyal Karzbrun, Alexandra M. Tayar, Vincent Noireaux, and Roy H. Bar-Ziv. Programmable on-chip dna compartments as artificial cells. *Science*, 345(6198):829–832, 2014. doi: 10.1126/science.1255550. URL http://www.sciencemag.org/content/345/6198/829.abstract.

[55] Salma Kassem, Thomas van Leeuwen, Anouk S. Lubbe, Miriam R. Wilson, Ben L. Feringa, and David A. Leigh. Artificial molecular motors. *Chemical Society Reviews*, 46(9):2592–2621, 2017. ISSN 0306-0012. doi: 10.1039/C7CS00245A. URL http://dx.doi.org/10.1039/C7CS00245A.

[56] Felix C. Keber, Etienne Loiseau, Tim Sanchez, Stephen J. DeCamp, Luca Giomi, Mark J. Bowick, M. Cristina Marchetti, Zvonimir Dogic, and

Andreas R. Bausch. Topology and dynamics of active nematic vesicles. *Science*, 345(6201):1135–1139, 2014. doi: 10.1126/science.1254784. URL https://www.ncbi.nlm.nih.gov/pmc/articles/PMC4401068/pdf/nihms676668.pdf.

[57] Jakia Jannat Keya, Ryuhei Suzuki, Arif Md. Rashedul Kabir, Daisuke Inoue, Hiroyuki Asanuma, Kazuki Sada, Henry Hess, Akinori Kuzuya, and Akira Kakugo. Dna-assisted swarm control in a biomolecular motor system. *Nature Communications*, 9(1):453, 2018. doi: 10.1038/s41467-017-02778-5. URL https://doi.org/10.1038/s41467-017-02778-5.

[58] A. J. Koch and H. Meinhardt. Biological pattern formation: from basic mechanisms to complex structures. *Reviews of Modern Physics*, 66(4):1481–1507, 1994. URL http://link.aps.org/doi/10.1103/RevModPhys.66.1481. RMP.

[59] Shigeru Kondo and Rihito Asai. A reaction-diffusion wave on the skin of the marine angelfish pomacanthus. *Nature*, 376:765 EP –, 08 1995. URL http://dx.doi.org/10.1038/376765a0.

[60] Shigeru Kondo and Takashi Miura. Reaction-diffusion model as a framework for understanding biological pattern formation. *Science*, 329(5999): 1616–1620, 2010.

[61] S. J. Kron and J. A. Spudich. Fluorescent actin filaments move on myosin fixed to a glass surface. *Proceedings of the National Academy of Sciences of the United States of America*, 83(17):6272–6276, 1986. ISSN 0027-8424 1091-6490. doi: 10.1073/pnas.83.17.6272. URL https://www.ncbi.nlm.nih.gov/pubmed/3462694

https://www.ncbi.nlm.nih.gov/pmc/articles/PMC386485/. 3462694[pmid] PMC386485[pmcid].

[62] K. Kruse, J. Joanny, F. Jülicher, J. Prost, and K. Sekimoto. Generic theory of active polar gels: a paradigm for cytoskeletal dynamics. *Eur. Phys. J. E*, 16:5–16, 2005. doi: 10.1140/epje/e2005-00002-5.

[63] Karsten Kruse, Jean-François Joanny, Frank Jülicher, Jacques Prost, and Ken Sekimoto. Asters, vortices, and rotating spirals in active gels of polar filaments. *Physical review letters*, 92(7):078101, 2004.

[64] Nitin Kumar, Rui Zhang, Juan J. de Pablo, and Margaret L. Gardel. Tunable structure and dynamics of active liquid crystals. *Science Advances*, 4(10), 2018. URL http://advances.sciencemag.org/content/4/10/eaat7779.abstract.

[65] Danielle Lebrecht, Marisa Foehr, Eric Smith, Francisco J. P. Lopes, Carlos E. Vanario-Alonso, John Reinitz, David S. Burz, and Steven D. Hanes. Bicoid cooperative dna binding is critical for embryonic patterning in drosophila. *Proceedings of the National Academy of Sciences of the United States of America*, 102(37): 13176–13181, 2005. ISSN 0027-8424 1091-6490. doi: 10.1073/pnas.0506462102. URL https://www.ncbi.nlm.nih.gov/pubmed/16150708 https://www.ncbi.nlm.nih.gov/pmc/articles/PMC1201621/.

[66] I. Lengyel and I. R. Epstein. Modeling of turing structures in the chlorite iodide malonic-acid starch reaction system. *Science*, 251(4994):650–652, 1991. ISSN 0036-8075. doi: 10.1126/science.251.4994.650.

[67] I Lengyel and I R Epstein. A chemical approach to designing tur-

ing patterns in reaction-diffusion systems. *Proc. Natl. Acad. Sci. U.S.A.*, 89(9):3977–3979, 1992. doi: 10.1073/pnas.89.9.3977. URL http://www.pnas.org/content/89/9/3977.abstract.

[68] I. Lengyel and I. R. Epstein. Turing structures in simple chemical-reactions. *Acc. Chem. Res.*, 26(5):235–240, 1993. ISSN 0001-4842. doi: 10.1021/ar00029a002. URL <Go to ISI>://WOS:A1993LC61000002.

[69] Quan Li, Gad Fuks, Emilie Moulin, Mounir Maaloum, Michel Rawiso, Igor Kulic, Justin T. Foy, and Nicolas Giuseppone. Macroscopic contraction of a gel induced by the integrated motion of light-driven molecular motors. *Nature Nanotechnology*, 10(2):161–165, 2015. ISSN 1748-3395. doi: 10.1038/nnano.2014.315. URL https://doi.org/10.1038/nnano.2014.315.

[70] Laurent Limozin and Erich Sackmann. Polymorphism of cross-linked actin networks in giant vesicles. *Physical Review Letters*, 89(16):168103, 2002. doi: 10.1103/PhysRevLett.89.168103. URL https://link.aps.org/doi/10.1103/PhysRevLett.89.168103. PRL.

[71] Thomas Litschel, Beatrice Ramm, Roel Maas, Michael Heymann, and Petra Schwille. Beating vesicles: Encapsulated protein oscillations cause dynamic membrane deformations. *Angewandte Chemie International Edition*, 57(50):16286–16290, 2018. ISSN 1433-7851. doi: 10.1002/anie.201808750. URL https://doi.org/10.1002/anie.201808750.

[72] Yan-Jun Liu, Mal LeBerre, Franziska Lautenschlaeger, Paolo Maiuri, Andrew Callan-Jones, Mélina Heuzé, Tohru Takaki, Raphal Voituriez, and Matthieu Piel. Confinement and low adhesion induce fast amoeboid

migration of slow mesenchymal cells. *Cell*, 160(4):659–672, 2015. ISSN 0092-8674. doi: https://doi.org/10.1016/j.cell.2015.01.007. URL http://www.sciencedirect.com/science/article/pii/S0092867415000082.

[73] Yifeng Liu, Yongxing Guo, James M. Valles, and Jay X. Tang. Microtubule bundling and nested buckling drive stripe formation in polymerizing tubulin solutions. *Proceedings of the National Academy of Sciences*, 103:10654–10659, 2006.

[74] Etienne Loiseau, Jochen A. M. Schneider, Felix C. Keber, Carina Pelzl, Gladys Massiera, Guillaume Salbreux, and Andreas R. Bausch. Shape remodeling and blebbing of active cytoskeletal vesicles. *Science Advances*, 2(4):e1500465, 2016. doi: 10.1126/sciadv.1500465. URL http://advances.sciencemag.org/content/2/4/e1500465.abstract.

[75] Martin Loose, Elisabeth Fischer-Friedrich, Jonas Ries, Karsten Kruse, and Petra Schwille. Spatial regulators for bacterial cell division self-organize into surface waves in vitro. *Science*, 320(5877):789–792, 2008.

[76] Martin Loose, Karsten Kruse, and Petra Schwille. Protein self-organization: Lessons from the min system. *Annual Review of Biophysics*, 40(1):315–336, 2011. ISSN 1936-122X. doi: 10.1146/annurev-biophys-042910-155332. URL http://dx.doi.org/10.1146/annurev-biophys-042910-155332.

[77] F. J. Lopes, F. M. Vieira, D. M. Holloway, P. M. Bisch, and A. V. Spirov. Spatial bistability generates hunchback expression sharpness in the drosophila embryo. *PLoS Comput. Biol.*, 4(9):e1000184, 2008. ISSN 1553-7358 (Electronic) 1553-734X (Linking). doi: 10.1371/journal.pcbi.1000184. URL http://www.ncbi.nlm.nih.gov/pubmed/18818726.

[78] Alfred J. Lotka. Undamped oscillations derived from the law of mass action. *Journal of the American Chemical Society*, 42(8):1595–1599, 1920. ISSN 0002-7863. doi: 10.1021/ja01453a010. URL https://doi.org/10.1021/ja01453a010 https://pubs.acs.org/doi/abs/10.1021/ja01453a010.

[79] M. C. Marchetti, J. F. Joanny, S. Ramaswamy, T. B. Liverpool, J. Prost, Madan Rao, and R. Aditi Simha. Hydrodynamics of soft active matter. *Reviews of Modern Physics*, 85(3):1143–1189, 2013. URL https://link.aps.org/doi/10.1103/RevModPhys.85.1143.

[80] Luciano Marcon, Xavier Diego, James Sharpe, and Patrick Müller. High-throughput mathematical analysis identifies turing networks for patterning with equally diffusing signals. *eLife*, 5:e14022, apr 2016. ISSN 2050-084X. doi: 10.7554/eLife.14022. URL https://dx.doi.org/10.7554/eLife.14022.

[81] Berta Martnez-Prat, Jordi Ignés-Mullol, Jaume Casademunt, and Francesc Sagués. Selection mechanism at the onset of active turbulence. *Nature Physics*, 2019. ISSN 1745-2481. doi: 10.1038/s41567-018-0411-6. URL https://doi.org/10.1038/s41567-018-0411-6.

[82] Eriko Sato Matsuo and Toyoichi Tanaka. Patterns in shrinking gels. *Nature*, 358(6386):482–485, 1992. ISSN 1476-4687. doi: 10.1038/358482a0. URL https://doi.org/10.1038/358482a0.

[83] Hans Meinhardt. Turing's theory of morphogenesis of 1952 and the subsequent discovery of the crucial role of local self-enhancement and long-range inhibition. *Interface Fo-*

cus, 2(4):407–416, 2012. doi: 10.1098/rsfs.2011.0097. URL http://rsfs.royalsocietypublishing.org/content/2/4/407.abstract.

[84] Jonathan B. Michaux, Franois B. Robin, William M. McFadden, and Edwin M. Munro. Excitable rhoa dynamics drive pulsed contractions in the early ¡em¿c. elegans¡/em¿ embryo. *The Journal of Cell Biology*, 217: 4230–4252, 2018.

[85] Tim Mitchison and Marc Kirschner. Dynamic instability of microtubule growth. *Nature*, 312(5991):237–242, 1984. ISSN 1476-4687. doi: 10.1038/312237a0. URL https://doi.org/10.1038/312237a0.

[86] H. Miyata and H. Hotani. Morphological changes in liposomes caused by polymerization of encapsulated actin and spontaneous formation of actin bundles. *Proceedings of the National Academy of Sciences of the United States of America*, 89(23):11547–11551, 1992. ISSN 0027-8424 1091-6490. doi: 10.1073/pnas.89.23.11547. URL https://www.ncbi.nlm.nih.gov/pubmed/1454846 https://www.ncbi.nlm.nih.gov/pmc/articles/PMC50589/ https://www.pnas.org/content/pnas/89/23/11547.full.pdf. 1454846[pmid] PMC50589[pmcid].

[87] Kevin Montagne, Raphael Plasson, Yasuyuki Sakai, Teruo Fujii, and Yannick Rondelez. Programming an in vitro dna oscillator using a molecular networking strategy. *Mol. Syst. Biol.*, 7:466, 2011.

[88] Kevin Montagne, Guillaume Gines, Teruo Fujii, and Yannick Rondelez. Boosting functionality of synthetic dna circuits with tailored deactivation. *Nat. Comm.*, 7:13474, 2016.

[89] Edwin Munro, Jeremy Nance, and James R. Priess. Cortical flows powered by asymmetrical contraction transport par proteins to establish and maintain anterior-posterior polarity in the early c. elegans embryo. *Developmental Cell*, 7(3):413–424, 2004. ISSN 1534-5807. doi: https://doi.org/10.1016/j.devcel.2004.08.001. URL http://www.sciencedirect.com/science/article/pii/S153458070400276X.

[90] Stefan Münster, Akanksha Jain, Alexander Mietke, Anastasios Pavlopoulos, Stephan W. Grill, and Pavel Tomancak. Attachment of the blastoderm to the vitelline envelope affects gastrulation of insects. *Nature*, 568 (7752):395–399, 2019. ISSN 1476-4687. doi: 10.1038/s41586-019-1044-3. URL https://doi.org/10.1038/s41586-019-1044-3.

[91] J. D. Murray. Parameter space for turing instability in reaction diffusion mechanisms: A comparison of models. *J. Theor. Biol.*, 98(1):143–163, 1982. ISSN 0022-5193. doi: 10.1016/0022-5193(82)90063-7. URL http://www.sciencedirect.com/science/article/pii/0022519382900637.

[92] J.D. Murray. *Mathematical Biology II :Spatial Models and Biomedical Applications*. Springer, New York, 2003.

[93] F. J. Nédélec, T. Surrey, A. C. Maggs, and S. Leibler. Self-organization of microtubules and motors. *Nature*, 389(6648):305–308, 1997. ISSN 0028-0836. URL http://dx.doi.org/10.1038/38532.

[94] Daniel Needleman and Zvonimir Dogic. Active matter at the interface between materials science and cell biology. *Nature reviews Materials*, 2:17048—17048, 2017. URL http://dx.doi.org/10.1038/natrevmats.2017.48.

[95] Daniel J. Needleman, Miguel A. Ojeda-Lopez, Uri Raviv, Kai Ewert, Jayna B. Jones, Herbert P. Miller, Leslie Wilson, and Cyrus R. Safinya. Synchrotron x-ray diffraction study of microtubules buckling and bundling under osmotic stress: A probe of interprotofilament interactions. *Physical Review Letters*, 93 (19):198104, 2004. doi: 10.1103/PhysRevLett.93.198104. URL https://link.aps.org/doi/10.1103/PhysRevLett.93.198104 https://journals.aps.org/prl/pdf/10.1103/PhysRevLett.93.198104 https://journals.aps.org/prl/abstract/10.1103/PhysRevLett.93.198104. PRL.

[96] Henrike Niederholtmeyer, Viktoria Stepanova, and Sebastian J. Maerkl. Implementation of cell-free biological networks at steady state. *Proceedings of the National Academy of Sciences*, 110(40):15985–15990, 2013. ISSN 0027-8424. doi: 10.1073/pnas.1311166110. URL https://www.pnas.org/content/110/40/15985.

[97] Lars Onsager. Reciprocal relations in irreversible processes. i. *Physical Review*, 37(4):405–426, 1931. doi: 10.1103/PhysRev.37.405. URL https://link.aps.org/doi/10.1103/PhysRev.37.405. PR.

[98] Achini Opathalage, Michael M. Norton, Michael P. N. Juniper, Blake Langeslay, S. Ali Aghvami, Seth Fraden, and Zvonimir Dogic. Self-organized dynamics and the transition to turbulence of confined active nematics. *Proceedings of the National Academy of Sciences*, 116(11): 4788–4797, 2019. ISSN 0027-8424. doi: 10.1073/pnas.1816733116. URL https://www.pnas.org/content/116/11/4788.

[99] H. G. Othmer and L. E. Scriven. Interactions of reaction and diffusion

in open systems. *Industrial & Engineering Chemistry Fundamentals*, 8 (2):302–313, 1969. ISSN 0196-4313. doi: 10.1021/i160030a020. URL http://dx.doi.org/10.1021/i160030a020.

[100] Adrien Padirac, Teruo Fujii, and Yannick Rondelez. Bottom-up construction of in vitro switchable memories. *Proc. Natl. Acad. Sci. U.S.A.*, 10.1073/pnas.1212069109, 2012.

[101] Adrien Padirac, Teruo Fujii, André Estévez-Torres, and Yannick Rondelez. Spatial waves in synthetic biochemical networks. *J. Am. Chem. Soc.*, 135(39):14586–14592, 2013.

[102] M. Pinot, F. Chesnel, J. Z. Kubiak, I. Arnal, F. J. Nedelec, and Z. Gueroui. Effects of confinement on the self-organization of microtubules and motors. *Current Biology*, 19(11):954–960, 2009. ISSN 0960-9822. doi: 10.1016/j.cub.2009.04.027. URL https://doi.org/10.1016/j.cub.2009.04.027.

[103] Léa-Laetitia Pontani, Jasper van der Gucht, Guillaume Salbreux, Julien Heuvingh, Jean-Franois Joanny, and Cécile Sykes. Reconstitution of an actin cortex inside a liposome. *Biophysical Journal*, 96(1):192–198, 2009. ISSN 0006-3495. doi: https://doi.org/10.1016/j.bpj.2008.09.029. URL http://www.sciencedirect.com/science/article/pii/S0006349508000386.

[104] C. Quininao, A. Prochiantz, and J. Touboul. Local homeoprotein diffusion can stabilize boundaries generated by graded positional cues. *Development*, 142(10):1860–8, 2015. ISSN 1477-9129 (Electronic) 0950-1991 (Linking). doi: 10.1242/dev.113688. URL http://www.ncbi.nlm.nih.gov/pubmed/25968317.

[105] David M. Raskin and Piet A. J. de Boer. Rapid pole-to-pole oscillation of a protein required for directing division to the middle of escherichia coli. *Proc. Natl. Acad. Sci. U.S.A.*, 96(9):4971–4976, 1999. doi: 10.1073/pnas.96.9.4971. URL `http://www.pnas.org/content/96/9/4971.abstract` `http://www.pnas.org/content/96/9/4971.full.pdf`.

[106] Johanna Roostalu, Jamie Rickman, Claire Thomas, Franois Nédélec, and Thomas Surrey. Determinants of polar versus nematic organization in networks of dynamic microtubules and mitotic motors. *Cell*, 175(3):796–808.e14, 2018. ISSN 0092-8674.

[107] Steffen Rulands, Ben Klünder, and Erwin Frey. Stability of localized wave fronts in bistable systems. *Phys. Rev. Lett.*, 110(3):038102, 2013.

[108] T. Sanchez, D. T. Chen, S. J. DeCamp, M. Heymann, and Z. Dogic. Spontaneous motion in hierarchically assembled active matter. *Nature*, 491(7424):431–4, 2012. ISSN 1476-4687 (Electronic) 0028-0836 (Linking). doi: 10.1038/nature11591. URL `http://www.ncbi.nlm.nih.gov/pubmed/23135402`.

[109] Tim Sanchez, Daniel T. N. Chen, Stephen J. DeCamp, Michael Heymann, and Zvonimir Dogic. Spontaneous motion in hierarchically assembled active matter, 2013.

[110] Yusuke Sato, Yuichi Hiratsuka, Ibuki Kawamata, Satoshi Murata, and Shin-ichiro M. Nomura. Micrometer-sized molecular robot changes its shape in response to signal molecules. *Science Robotics*, 2, 2017.

[111] Volker Schaller, Christoph Weber, Christine Semmrich, Erwin Frey, and Andreas R. Bausch. Polar patterns of driven fila-

ments. *Nature*, 467:73, 2010. doi: 10.1038/nature09312https://www.nature.com/articles/nature09312#supplementary-information. URL https://doi.org/10.1038/nature09312.

[112] Natalie S. Scholes and Mark Isalan. A three-step framework for programming pattern formation. *Current Opinion in Chemical Biology*, 40:1 – 7, 2017. ISSN 1367-5931. doi: https://doi.org/10.1016/j.cbpa.2017.04.008. URL http://www.sciencedirect.com/science/article/pii/S1367593117300108.

[113] Anis Senoussi, Shunnichi Kashida, Raphaël Voituriez, Jean-Christophe Galas, Ananyo Maitra, and André Estévez-Torres. Tunable corrugated patterns in an active nematic sheet. *Proceedings of the National Academy of Sciences*, 116(45):22464–22470, 2019.

[114] Rushikesh Sheth, Luciano Marcon, M. Félix Bastida, Marisa Junco, Laura Quintana, Randall Dahn, Marie Kmita, James Sharpe, and Maria A. Ros. Hox genes regulate digit patterning by controlling the wavelength of a turing-type mechanism. *Science*, 338 (6113):1476–1480, 2012. doi: 10.1126/science.1226804. URL http://www.sciencemag.org/content/338/6113/1476.abstract http://www.ncbi.nlm.nih.gov/pmc/articles/PMC4486416/pdf/nihms4759.pdf.

[115] Stephen Smith and Neil Dalchau. Model reduction enables turing instability analysis of large reaction–diffusion models. *Journal of The Royal Society Interface*, 15(140), 2018. ISSN 1742-5689. doi: 10.1098/rsif.2017.0805. URL http://rsif.royalsocietypublishing.org/content/15/140/20170805.

[116] Mohammad Soheilypour, Mohaddeseh Peyro, StephenJ Peter, and

MohammadR K. Mofrad. Buckling behavior of individual and bundled microtubules. *Biophysical Journal*, 108(7):1718–1726, 2015. ISSN 0006-3495. doi: https://doi.org/10.1016/j.bpj.2015.01.030. URL http://www.sciencedirect.com/science/article/pii/S0006349515001241.

[117] Niranjan Srinivas, James Parkin, Georg Seelig, Erik Winfree, and David Soloveichik. Enzyme-free nucleic acid dynamical systems. *Science*, 358, 2017.

[118] Yutaka Sumino, Ken H. Nagai, Yuji Shitaka, Dan Tanaka, Kenichi Yoshikawa, Hugues Chaté, and Kazuhiro Oiwa. Large-scale vortex lattice emerging from collectively moving microtubules. *Nature*, 483:448, 2012. doi: 10.1038/nature10874https://www.nature.com/articles/nature10874#supplementary-information. URL https://doi.org/10.1038/nature10874.

[119] Thomas Surrey, Francois Nédélec, Stanislas Leibler, and Eric Karsenti. Physical properties determining self-organization of motors and microtubules. *Science*, 292 (5519):1167–1171, 2001. doi: 10.1126/science.1059758. URL http://science.sciencemag.org/content/292/5519/1167.long.

[120] J. Tabony and D. Job. Spatial structures in microtubular solutions requiring a sustained energy source. *Nature*, 346(6283):448–451, 1990. URL http://dx.doi.org/10.1038/346448a0. 10.1038/346448a0.

[121] Kingo Takiguchi, Ayako Yamada, Makiko Negishi, Yohko Tanaka-Takiguchi, and Kenichi Yoshikawa. Entrapping desired amounts of actin filaments and molecular motor proteins in giant liposomes. *Langmuir*, 24

(20):11323–11326, 2008. ISSN 0743-7463. doi: 10.1021/la802031n. URL https://doi.org/10.1021/la802031n.

[122] Ruensern Tan, Peter J. Foster, Daniel J. Needleman, and Richard J. McKenney. Cooperative accumulation of dynein-dynactin at microtubule minus-ends drives microtubule network reorganization. *Developmental Cell*, 44(2):233–247.e4, 2018. ISSN 1534-5807. doi: https://doi.org/10.1016/j.devcel.2017.12.023. URL http://www.sciencedirect.com/science/article/pii/S1534580717310407.

[123] Alexandra M. Tayar, Eyal Karzbrun, Vincent Noireaux, and Roy H. Bar-Ziv. Synchrony and pattern formation of coupled genetic oscillators on a chip of artificial cells. *Proceedings of the National Academy of Sciences*, 114(44):11609–11614, 2017. doi: 10.1073/pnas.1710620114. URL http://www.pnas.org/content/pnas/114/44/11609.full.pdf.

[124] Akanksha Thawani, Howard A. Stone, Joshua W. Shaevitz, and Sabine Petry. Spatiotemporal organization of branched microtubule networks. *eLife*, 8:e43890, 2019. ISSN 2050-084X. doi: 10.7554/eLife.43890. URL https://doi.org/10.7554/eLife.43890.

[125] Nathan Tompkins, Ning Li, Camille Girabawe, Michael Heymann, G. Bard Ermentrout, Irving R. Epstein, and Seth Fraden. Testing turing's theory of morphogenesis in chemical cells. *Proc. Natl. Acad. Sci. U.S.A.*, 10.1073/pnas.1322005111, 2014. doi: 10.1073/pnas.1322005111. URL http://www.pnas.org/content/early/2014/03/05/1322005111.abstract.

[126] Takayuki Torisawa, Daisuke Taniguchi, Shuji Ishihara, and Kazuhiro Oiwa. Spontaneous formation of a globally connected contractile

network in a microtubule-motor system. *Biophysical journal*, 111 (2):373–385, 2016. ISSN 1542-0086 0006-3495. doi: 10.1016/j.bpj.2016.06.010. URL https://www.ncbi.nlm.nih.gov/pubmed/27463139 https://www.ncbi.nlm.nih.gov/pmc/PMC4968425/.

[127] Feng-Ching Tsai, Bjrn Stuhrmann, and Gijsje H. Koenderink. Encapsulation of active cytoskeletal protein networks in cell-sized liposomes. *Langmuir*, 27(16):10061–10071, 2011. ISSN 0743-7463. doi: 10.1021/la201604z. URL https://doi.org/10.1021/la201604z.

[128] A. J. Turberfield, J. C. Mitchell, B. Yurke, Jr. Mills, A. P., M. I. Blakey, and F. C. Simmel. DNA fuel for free-running nanomachines. *Phys. Rev. Lett.*, 90(11):118102, 2003.

[129] A. Turing. The chemical basis of morphogenesis. *Bull. Math. Biol.*, 52 (1):153–197, 1990.

[130] A. M. Turing. The chemical basis of morphogenesis. *Philos. Trans. R. Soc. Lond. B. Biol. Sci.*, 237(641):37–72, 1952.

[131] Georg Urtel, André Estevez-Torres, and Jean-Christophe Galas. Dna-based long-lived reaction-diffusion patterning in a host hydrogel. *Soft Matter*, in press, 2019.

[132] Georg Urtel, Marc Van Der Hofstadt, Jean-Christophe Galas, and André Estevez-Torres. rexpar: An isothermal amplification scheme that is robust to autocatalytic parasites. *Biochemistry*, 58(23):2675–2681, 2019.

[133] R. D. Vale, T. S. Reese, and M. P. Sheetz. Identification of a novel force-generating protein, kinesin, involved in microtubule-based motility. *Cell*, 42(1):39–50, 1985. ISSN

0092-8674 1097-4172. doi: 10.1016/s0092-8674(85)80099-4. URL https://www.ncbi.nlm.nih.gov/pubmed/3926325 https://www.ncbi.nlm.nih.gov/pmc/articles/PMC2851632/. 3926325[pmid] PMC2851632[pmcid] S0092-8674(85)80099-4[PII].

[134] Ronald D. Vale. The molecular motor toolbox for intracellular transport. *Cell*, 112(4):467–480, 2003. ISSN 0092-8674.

[135] Ronald D. Vale, Bruce J. Schnapp, Thomas S. Reese, and Michael P. Sheetz. Organelle, bead, and microtubule translocations promoted by soluble factors from the squid giant axon. *Cell*, 40(3):559–569, 1985. ISSN 0092-8674. doi: https://doi.org/10.1016/0092-8674(85)90204-1. URL http://www.sciencedirect.com/science/article/pii/0092867485902041.

[136] Marc; Van Der Hofstadt, Guillaume; Gines, Jean-Christophe; Galas, and André Estevez-Torres. Programming spatio-temporal patterns with dna-based circuits. In K. Evgeny, editor, *DNA- and RNA-Based Computing Systems*. Wiley VCH, in press.

[137] V. K. Vanag and I. R. Epstein. Inwardly rotating spiral waves in a reaction-diffusion system. *Science*, 294(5543):835–837, 2001. ISSN 0036-8075. doi: 10.1126/science.1064167. URL <Go to ISI>://WOS:000171851800041.

[138] V. K. Vanag and I. R. Epstein. Segmented spiral waves in a reaction-diffusion system. *Proc. Natl. Acad. Sci. U. S. A.*, 100(25):14635–14638, 2003. ISSN 0027-8424. doi: 10.1073/pnas.2534816100. URL <Go to ISI>://WOS:000187227200008.

[139] Vladimir K. Vanag and Irving R. Epstein. Pattern formation in

a tunable medium: The belousov-zhabotinsky reaction in an aerosol ot microemulsion. *Phys. Rev. Lett.*, 87(22):228301, 2001. URL http://link.aps.org/doi/10.1103/PhysRevLett.87.228301.

[140] Gabriel Villar, Alexander D. Graham, and Hagan Bayley. A tissue-like printed material. *Science*, 340 (6128):48–52, 2013. doi: 10.1126/science.1229495. URL http://www.sciencemag.org/content/340/6128/48.abstract.

[141] R. Voituriez, J. F. Joanny, and J. Prost. Spontaneous flow transition in active polar gels. *Europhysics Letters (EPL)*, 70(3):404–410, 2005. ISSN 0295-5075 1286-4854. doi: 10.1209/epl/i2004-10501-2. URL http://dx.doi.org/10.1209/epl/i2004-10501-2 https://iopscience.iop.org/article/10.1209/epl/i2004-10501-2/pdf https://iopscience.iop.org/article/10.1209/epl/i2004-10501-2/meta.

[142] Vito Volterra. Fluctuations in the abundance of a species considered mathematically1. *Nature*, 118:558, 1926. doi: 10.1038/118558a0. URL http://dx.doi.org/10.1038/118558a0 http://www.nature.com/articles/118558a0.pdf.

[143] Siyuan S. Wang and Andrew D. Ellington. Pattern generation with nucleic acid chemical reaction networks. *Chemical Reviews*, 119(10):6370–6383, 2019.

[144] Kimberly L. Weirich, Kinjal Dasbiswas, Thomas A. Witten, Suriyanarayanan Vaikuntanathan, and Margaret L. Gardel. Self-organizing motors divide active liquid droplets. *Proceedings of the National Academy of Sciences*, 116:11125–11130, 2019.

[145] Viktoria Wollrab, Julio M. Belmonte, Lucia Baldauf, Maria Leptin, Franois Nédeléc, and Gijsje H. Koenderink. Polarity sorting drives remodeling of actin-myosin networks. *Journal of Cell Science*, 132(4):jcs219717, 2019. doi: 10.1242/jcs.219717. URL http://jcs.biologists.org/content/132/4/jcs219717.abstract https://jcs.biologists.org/content/joces/132/4/jcs219717.full.pdf.

[146] C. Wolpert, L.; Tickle. *Principles of development*. Oxford University Press, Oxford, 2011.

[147] L. Wolpert. Positional information and the spatial pattern of cellular differentiation. *J. Theor. Biol.*, 25(1):1–47, 1969.

[148] Kun-Ta Wu, Jean Bernard Hishamunda, Daniel T. N. Chen, Stephen J. DeCamp, Ya-Wen Chang, Alberto Fernndez-Nieves, Seth Fraden, and Zvonimir Dogic. Transition from turbulent to coherent flows in confined three-dimensional active fluids. *Science*, 355(6331), 2017. URL http://science.sciencemag.org/content/355/6331/eaal1979.abstract.

[149] Motoomi Yamaguchi, Eiichi Yoshimoto, and Shigeru Kondo. Pattern regulation in the stripe of zebrafish suggests an underlying dynamic and autonomous mechanism. *Proceedings of the National Academy of Sciences*, 104(12):4790, 03 2007. URL http://www.pnas.org/content/104/12/4790.abstract.

[150] Ryo Yoshida and Takeshi Ueki. Evolution of self-oscillating polymer gels as autonomous polymer systems. *NPG Asia Mater*, 6:e107, 2014. doi: 10.1038/am.2014.32. URL http://dx.doi.org/10.1038/am.2014.32 http://www.nature.com/am//journal/v6/n6/pdf/am201432a.pdf.

[151] Ryo Yoshida, Toshikazu Takahashi, Tomohiko Yamaguchi, and Hisao Ichijo. Self-oscillating gel. *J. Am. Chem. Soc.*, 118(21):5134–5135, 1996. ISSN 0002-7863. doi: 10.1021/ja9602511. URL `http://dx.doi.org/10.1021/ja9602511`.

[152] Bernard Yurke, Andrew J. Turberfield, Allen P. Mills, Friedrich C. Simmel, and Jennifer L. Neumann. A dna-fuelled molecular machine made of dna. *Nature*, 406(6796):605–608, 2000.

[153] Anton S. Zadorin, Yannick Rondelez, Jean-Christophe Galas, and Andre Estevez-Torres. Synthesis of programmable reaction-diffusion fronts using dna catalyzers. *Phys. Rev. Lett.*, 114(6):068301, 2015.

[154] Anton S. Zadorin, Yannick Rondelez, Guillaume Gines, Vadim Dilhas, Georg Urtel, Adrian Zambrano, Jean-Christophe Galas, and André Estevez-Torres. Synthesis and materialization of a reaction-diffusion french flag pattern. *Nature Chemistry*, 9:990, 2017.

[155] A. Zambrano, A. S. Zadorin, Y. Rondelez, A. Estévez-Torres, and J. C. Galas. Pursuit-and-evasion reaction-diffusion waves in microreactors with tailored geometry. *The Journal of Physical Chemistry B*, 119(17): 5349–5355, 2015.

[156] John Zenk, Dominic Scalise, Kaiyuan Wang, Phillip Dorsey, Joshua Fern, Ariana Cruz, and Rebecca Schulman. Stable dna-based reaction-diffusion patterns. *RSC Adv.*, 7:18032–18040, 2017.

[157] D. Y. Zhang and E. Winfree. Control of dna strand displacement kinetics using toehold exchange. *J. Am. Chem. Soc.*, 131(47):17303–14, 2009.

[158] David Yu Zhang and Georg Seelig. Dynamic dna nanotechnology using strand-displacement reactions. *Nat Chem*, 3(2):103–113, 2011.

[159] Rui Zhang, Ye Zhou, Mohammad Rahimi, and Juan J. de Pablo. Dynamic structure of active nematic shells. *Nature Communications*, 7 (1):13483, 2016. ISSN 2041-1723. doi: 10.1038/ncomms13483. URL `https://doi.org/10.1038/ncomms13483`.